DETERMINATION OF THE NORMAL COMPONENT OF INDUCED VELOCITY IN THE FLOW FIELD OF A UNIFORMLY LOADED LIFTING ROTOR HOVERING IN GROUND EFFECT BY USE OF AN ELECTROMAGNETIC-ANALOG AND A METHOD FOR UTILIZING THIS INFORMATION TO CALCULATE INTERFERENCE INDUCED VELOCITIES FOR MULTI-ROTOR HELICOPTERS

A THESIS

Presented to

the Faculty of the Graduate Division

by

Grayson D. Tate, Jr.

In Partial Fulfillment

of the Requirements for the Degree

Master of Science in Aeronautical Engineering

Georgia Institute of Technology

August, 1958

"In presenting the dissertation as a partial fulfillment of the requirements for an advanced degree from the Georgia Institute of Technology, I agree that the Library of the Institution shall make it available for inspection and circulation in accordance with its regulations governing materials of this type. I agree that permission to copy from, or to publish from, this dissertation may be granted by the professor under whose direction it was written, or, in his absence, by the dean of the Graduate Division when such copying or publication is solely for scholarly purposes and does not involve potential financial gain. It is understood that any copying from, or publication of, this dissertation which involves potential financial gain will not be allowed without written permission.

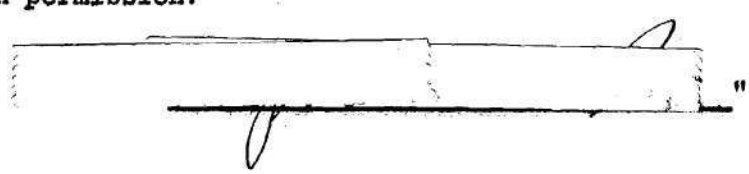

"

7A
12R

DETERMINATION OF THE NORMAL COMPONENT OF INDUCED VELOCITY IN THE FLOW FIELD OF A UNIFORMLY LOADED LIFTING ROTOR HOVERING IN GROUND EFFECT BY USE OF AN ELECTROMAGNETIC-ANALOG AND A METHOD FOR UTILIZING THIS INFORMATION TO CALCULATE INTERFERENCE INDUCED VELOCITIES FOR MULTI-ROTOR HELICOPTERS

Approved :

Walter Castles, Jr.

Robin B. Gray

Thomas W. Jackson

Date Approved by Chairman

ACKNOWLEDGEMENTS

I wish to express my most sincere appreciation to Professor Walter Castles, Jr. for suggesting the subject and for his valuable suggestions and guidance. I also want to thank Doctor Robin B. Gray and Doctor Thomas W. Jackson for their critical review of the topic.

TABLE OF CONTENTS

LIST OF TABLES

LIST OF FIGURES

Figure Page

LIST OF SYMBOLS

C_T	rotor thrust coefficient, $C_T = \dfrac{T}{\rho \pi \Omega^2 R^4}$
h/R	nondimensional distance of point P above or below the rotor plane
MR	output-meter reading, db
N	subscript for values at the normalizing point
P	subscript for values at an arbitrary point P in the rotor flow field
R	rotor radius
r/R	nondimensional radius measured to an arbitrary point P from the rotor axis
T	rotor thrust
v	normal component of induced velocity at center of the disc for $Z/R = \infty$, $v \approx \Omega R \sqrt{\frac{1}{2} C_T}$
V_i/v	nondimensional normal component of induced velocity at arbitrary point P, positive in downward direction
$(V_i/v)_i$	nondimensional interference induced velocity at arbitrary point P, positive in downward direction
x/R	nondimensional distance of point P above or below the source or sink plane
Z/R	nondimensional distance of disc above the ground plane
ϵ	an infinitesimal distance
ρ	density
ψ	azimuth angle of arbitrary point P, measured counterclockwise from the downwind position
Ω	angular velocity of the rotor

SUMMARY

This paper presents a method for determining the interference induced velocities for multi-rotor helicopters hovering in ground effect. The information required is provided in the form of tables and graphs, and shows the nondimensional normal component of induced velocity in the vicinity of a uniform vortex cylinder and its image. This information was obtained by measuring the magnetic field strength about an electromagnetic-analogy model of the wake vortex system. The tables and graphs give the nondimensional normal component of induced velocity for points in planes parallel to the tip-path plane and extending to six rotor radii from the wake centerline. The measurements covered the region extending 0.3 rotor radius above and below the tip-path plane, and were made for four different ground heights ranging from one-half to two rotor radii. For each ground height, the values were normalized to the point in the plane of the rotor at the wake centerline. The theoretical nondimensional normal component of induced velocity at each normalizing point was calculated from the Biot-Savart relation.

Physical interference between the field coils and the search coil made it impossible to obtain data at certain points by the experimental method employed. For these points, a mathematical procedure which employs uniform distributions of sources and sinks over circular discs, can be used to find the nondimensional normal component of induced velocity. An illustration of this procedure is provided.

Values of the nondimensional normal component of induced velocity along the rotor radius for each ground height are compared with the data obtained by Knight and Hefner in NACA TN 835.

A sample problem is worked out in order to show how the experimental and calculated data from this thesis can be utilized to find the interference induced velocities at points in the planes of both rotors of a typical tandem-rotor helicopter.

The method of superposition used in the sample problem can be extended to helicopters having three or more rotors.

CHAPTER I

INTRODUCTION

The calculation of the forces acting on the rotor of a helicopter requires a knowledge of the magnitude of the induced velocities in the vicinity of the rotor. These velocities are induced by the vortex system of the rotor itself in the case of a single-rotor helicopter, and they are supplemented by the velocities induced by the vortex systems of the other rotors for multi-rotor helicopters. The component of induced velocity normal to the plane of rotation is of particular interest, since it is this component on which the local angles of attack of the rotor blade elements are largely dependent.

If the complete induced velocity field of a rotor is known, it is possible to use the principle of superposition to calculate the induced velocity at points on the rotor discs of multi-rotor helicopters. This procedure assumes that there is no distortion of the individual wake vortex systems. However, a detailed knowledge of the geometric relations between the various rotors is required.

In reference 1, Knight and Hefner used a mathematical analysis to show the effect of the ground plane on the nondimensional induced velocity along the blade of a single hovering rotor. Because of the fact that their calculations were confined within the limits of the rotor disc, additional information was required for the region beyond the rotor tip before the principle of superposition mentioned above could be used.

The direct calculation of the induced velocity field for a rotor hovering in ground effect is lengthy since numerical integration is involved. Another approach is to make use of the perfect analogy between the induced flow associated with a vortex filament in a perfect fluid and the magnetic field in space associated with a current carrying wire. If an electromagnetic-analogy model of the wake vortex and image systems of a single rotor is made, the point measurements of the magnetic field strength of the associated magnetic field afford a description of the analogous induced velocity in the fluid velocity field. The latter method was the one employed to obtain the majority of the information contained in this thesis.

For certain points at which physical interference between the field coils and search coil made it impossible to measure the magnetic field strength, another procedure may be used to find the nondimensional normal component of induced velocity. In this procedure, uniform distributions of sources and sinks are placed over circular discs so that they duplicate the flow field of the uniform vortex cylinder. Values of the nondimensional normal component of induced velocity may then be calculated from the known flow fields of the source and sink distributions. An illustration of the procedure is provided.

In order to demonstrate how the experimental and calculated data might be used, a sample problem was included. In this problem, a typical tandem-rotor helicopter was assumed, and the nondimensional interference induced velocity determined at selected points in the planes of both rotors.

The analysis presented in the paper concerns the flow field associated with a uniformly loaded lifting rotor, and uses the assumption that the wake vortex system and its image have the form of uniform right circular cylinders composed of a very large number of circular vortex ring elements arranged in such a way that the circulation per unit length of the vortex sheet is constant.

CHAPTER II

APPARATUS AND EXPERIMENTAL PROCEDURE

The equipment used for the experimental portion of this thesis consisted essentially of four components :

1. Primary coil (wire model of wake vortex cylinder)
2. Secondary coil (search coil)
3. Amplifier and output meter
4. Power supply

The equipment was generally the same as that used in reference 2, the main exception being that the alternator in the power supply was driven by a synchronous motor.

The procedure used was essentially that of measuring the voltage induced in the secondary or search coil by the magnetic field which was produced by the current in the primary coil. These measurements were then converted into an equivalent velocity ratio.

Information in reference 2 indicates that the type of equipment used in the experimental work of this thesis is subject to certain inaccuracies, among which are :

1. Extraneous magnetic fields
2. Impure waveforms in the primary coil current
3. Induced effects in the primary coil and search coil leads
4. Search coil dimensions
5. Primary coil field distortion

In sections to follow, the description of each of the four basic components of equipment is given.

Primary field coil - The primary coil (wake model) was constructed by the use of lumped coils, each of which consisted of 18 turns of No. 17, Brown and Sharpe gage copper wire, wound about a Plexiglass coil form. Each of these coils was attached to an individual Plexiglass base which was fastened by means of nylon nuts and bolts to a heavy fiber base plate as shown in Figures 1 (a) and 1 (b). Each coil was oriented such that its face was perpendicular to the wake centerline. The spacing of the coils was uniform so that there were approximately 21 turns per inch of the model length, when measured along the wake centerline. A current of approximately four amperes flowed in the primary coil circuit for all tests. The coils were connected in series, the input and return wires being juxtaposed in order that they might be tightly twisted. This requirement necessitated a double coil winding, but minimized the external magnetic field of the leads of each individual coil. The wires connecting the power supply to the primary coils were also twisted for the same reason. The wake coils had an effective diameter of 12 inches between wire centers. The arrangement of the coils approximated a wake consisting of coaxial vortex rings arranged in the shape of a uniform vortex cylinder and the image of this cylinder below the ground plane. The direction of current flow in the image cylinder was opposite to that in the real cylinder. Figures 1 (a) and 1 (b) show two views of the model assembly, which was approximately centered in its containing room.

Search coil - Since the wake model magnetic field was nonlinear, the search coil had to be small in order to approximate point measurements in the primary coil magnetic field. The search coil was the same coil that was used for obtaining the experimental data in reference 2. This search coil had a diameter of approximately 0.35 inch to the center of its wire bundle. This diameter was about 3 percent of the primary coil diameter. The coil consisted of 1000 turns of No. 40, Brown and Sharpe gage, copper wire wound on a Plexiglass coil form which was fastened to a Plexiglass support. In order to simplify the positioning of the search coil, scribed lines were placed on the search coil support, the primary coil supporting table, and a vertical measuring platform. Calibration of the search coil circuit was not required, since the field strength measurements were normalized to points on the wake centerline for which values of the nondimensional normal component of induced velocity were calculated (Appendix I). The entire search coil assembly together with its coaxial connector is shown in Figure 2.

Amplifier and output-meter - The pickup circuit consisted of the search coil, its coaxial connector, and a commercial standing wave indicator. The standing wave indicator had a maximum sensitivity of 0.1 microvolt for full scale deflection, and consisted of an indicating meter, a high-gain 400 cycle fixed-frequency amplifier with a calibrated gain control covering a range of 60 decibels, and a narrow 400 cycle band-pass-filter having a sharp cut-off at 400 ± 5 cycles per second. The input impedance of the amplifier was 200,000 ohms, which was sufficient impedance to allow the foregoing of any meter scale calibration as discussed in reference 2. Figure 3 shows the standing wave indicator positioned in a

separate room from that of the field coils. Reference 2 indicates that this separation is necessary in order to eliminate direct magnetic coupling from the field coils.

Power supply - The power supply used for the wake model under discussion consisted of a 400 cycle aircraft alternator driven by a synchronous motor. Components in the circuit included an ammeter, voltmeter, capacitors, and variable resistors. The amount of capacitance was adjusted for each nondimensional ground height, Z/R, such that it approximately placed the circuit in a resonant condition. The variable resistors were adjusted to produce a current of approximately four amperes. Figure 4 shows the power supply assembly which was located in a separate room from those of the field coils and standing wave indicator so as to reduce direct magnetic coupling.

Field survey procedure - In order to obtain a stable condition, the primary coil circuit was given a minimum warm-up period of 45 minutes before any measurements were taken. Measurements were then made at the proper normalizing point in the plane of the rotor at the wake centerline for which the nondimensional normal component of induced velocity was calculated using the Biot-Savart relation. A separate normalizing point was necessary for each of the four nondimensional rotor heights (Z/R). The search coil circuit was renormalized at frequent intervals. For each value of Z/R, the magnetic field strength was measured at points along a line parallel to the rotor plane and extending from the axis of the wire model to a distance the equivalent of six rotor radii. Since the flow about a uniform vortex cylinder is axially symmetric, it was only necessary to obtain measurements in one radial plane. However, in order to have a check on the measurements, readings

were actually taken in two radial planes. One of these was parallel to the top of the field coil supporting table. The other was perpendicular to the supporting table and required the use of the vertical measuring platform which can be seen in Figures 1 (a) and 1 (b). Measurements were then taken covering the region extending 0.3 rotor radii above and below the rotor plane ($-0.3 < h/R < +0.3$). The figure $\pm$ 0.3 rotor radii was selected since the vertical rotor spacing of multi-rotor helicopters falls within these limits. The measurements described above were taken for each of the four nondimensional rotor heights, $Z/R = 0.5, 1.0, 1.5$, and 2.0.

Reduction of data - Since the output-meter was calibrated in decibels, it was necessary to convert the meter readings into equivalent values of the nondimensional normal component of induced velocity using the following formula :

$$\left|V_i/v\right|_P = \left|V_i/v\right|_N \left[\frac{\text{antilog } 0.1\,(MR)_P}{\text{antilog } 0.1\,(MR)_N}\right]$$

where V_i/v = nondimensional normal component of induced velocity

P = subscript referring to the space point at which measurements are made

N = subscript referring to the normalizing points for which computed values were known

A consideration of the flow field geometry and graphs of the experimental results made it possible to assign the proper sign to each value of V_i/v. The reduced data is shown in Table 1 and Figure 5.

A value for the normal component of induced velocity at the cen-

ter of the rotor, v, must be found in order to convert V_i/v into actual dimensional velocities at a point. Making the assumption that the relation between the thrust and the wake vortex sheet strength is only slightly affected by the presence of the ground plane, it follows that

$$v \approx \Omega R \sqrt{\tfrac{1}{2} C_T}$$

This is the usual approximation for the value of v out of ground effect ($Z/R = \infty$)

CHAPTER III

RESULTS

Tables 1 (a)-1(d) show the experimental results where, for each table, V_i/v is recorded for various values of r/R and h/R for a fixed nondimensional ground distance, Z/R. A separate table is provided for Z/R = 0.5, 1.0, 1.5, and 2.0. Figure 5 gives a graphical presentation of this same information in the region in which the values are significant.

Because of the physical interference between the primary and search coils, no data could be obtained in the plane of rotation (h/R = 0) between r/R = 0.9 and r/R = 1.1. Likewise, no data was obtained for r/R < 1.1 for planes below the plane of rotation (h/R < 0). For regions such as these in which no experimental values could be obtained, values of V_i/v may be calculated by the method shown in Appendix II. This method was used to calculate values of V_i/v at several of the selected sample points of the sample problem of Chapter IV, and the results of these calculations are shown in Table 2.

Figure 6 gives a comparison of the experimental results inside the wake in the plane of rotation with the mathematical results obtained by Knight and Hefner (1). It should be noted that the ordinate w_c/k used in reference 1 is one-half the value of V_i/v used in this paper. This comparison indicates that the accuracy of the experimental results of this paper should be satisfactory for engineering purposes. For points near the wake boundary (0.9 < r/R < 1.2), the gradient of

the local magnetic field strength was large, and it was not possible to get consistent meter readings on account of the fact that a very small change in location of the search coil caused appreciable variation in meter readings. At all other points in the flow field, repetition of the measurements gave no appreciable variation in meter readings. It is well to point out, however, that the uniform mathematical model used in reference 1 also necessitated certain approximations. Also, the computations yielding values of V_i/v near the edge of the wake in reference 1 required the use of only the first few terms of an infinite series of Legendre's Polynomials. With these facts in mind, it is only reasonable to conclude that neither the electromagnetic-analog nor the uniform mathematical model used by Knight and Hefner can be relied on for values of V_i/v near the edge of the rotor disc.

Chapter IV provides a method for utilizing the mathematical and calculated results of this paper to find the interference induced velocity distributions for multi-rotor helicopters. In the sample problem shown, the nondimensional interference induced velocity was determined at selected points in the planes of both rotors of a typical tandem-rotor helicopter shown in Figure 7. Figures 8 (a) and 8 (b), which show graphs of the nondimensional interference induced velocity $(V_i/v)_i$ vs r/R along various azimuth lines in the plane of each rotor, give the final nondimensional results.

CHAPTER IV

SAMPLE PROBLEM SHOWING THE CALCULATION OF INTERFERENCE INDUCED VELOCITIES AT SELECTED POINTS IN THE PLANE OF BOTH ROTORS OF A TYPICAL TANDEM-ROTOR HELICOPTER

For this sample problem, the helicopter was assumed to be hovering with its wheels 48 inches off the ground, and had the dimensions and general configuration shown in Figure 7. The sample points for which the nondimensional interference induced velocity was determined are located on lines radiating from the hub of each rotor at $\psi = 0^\circ$, 90° , 135° , 180° , 270° , and 315° , and are located at r/R = 0, 0.2, 0.4, 0.6, 0.8, and 1.0 along each of these lines.

It is noted that in this position with the wheels 48 inches off the ground, the front rotor is at a Z/R = 0.8, while the rear rotor is at a Z/R = 1.0. With respect to the front rotor, the rear rotor has an h/R = + 0.2. With respect to the rear rotor, the front rotor has an h/R = - 0.2.

The problem entailed the determination of graphs of $(V_i/v)_i$ vs r/R along the various azimuth lines mentioned above where, for each rotor, the appropriate Z/R and h/R were used. In order to accomplish this, it was necessary to use the original graphs of V_i/v vs r/R for the various values of Z/R and h/R as shown in Figure 5. In this sample problem, only the curves for h/R = $\pm$ 0.2 were of interest. In Figures 5 (b) and 5 (c), where no data was known for h/R = - 0.2, a linear interpolation was used between the experimental values for h/R = - 0.1 and h/R = - 0.3.

Utilizing data from the above graphs (Figure 5), a cross-plot was made showing V_i/v vs Z/R at constant r/R for $h/R = + 0.2$ and $h/R = - 0.2$ as shown in Figures 9 (a) and 9 (b). Figure 10 was plotted utilizing the information from Figure 9. One curve in Figure 10 shows V_i/v vs r/R at $Z/R = 1.0$, $h/R = - 0.2$ for points in the front rotor. To complete this graph, it was necessary to make use of the experimental information from Figure 9 as well as additional information from Table 2, which was calculated by utilizing uniform distributions of sources and sinks over circular discs. The calculated data gave the necessary information at points in the plane of the front rotor which were at locations in or near the rotor overlap region for which no experimental information was available. Seven of the sample points mentioned above were so located. The second curve in Figure 10 shows V_i/v vs r/R at $Z/R = 0.8$, $h/R = + 0.2$ for points in the rear rotor. With the two curves from Figure 10 available, it was then possible to find the nondimensional interference induced velocity at any point in the plane of either rotor.

Distances were then measured from the center of each rotor to the sample points in the plane of the opposite rotor by using a large scale plan view of the rotors of the helicopter. A small scale plan view is shown in Figure 11. With these distances expressed nondimensionally, Figure 10 was used to find the nondimensional normal component of induced velocity for all the sample points, as shown in Table 3. From the information in Table 3, graphs were made for each rotor showing $(V_i/v)_i$ vs r/R for each of the selected values of ψ as shown in Figures 8 (a) and 8 (b).

Once the nondimensional values of interference induced velocity are known, the approximate values for the dimensional velocities may be found by the relation :

$$(V_i)_i = \left[(V_i/v)_i\right](v)$$

where $$v \approx \Omega R \sqrt{\tfrac{1}{2}C_T} \qquad (Z/R = \infty)$$

As mentioned previously, the use of this formula requires the assumption that the relation between the thrust and the wake vortex sheet strength is only slightly affected by the presence of the ground plane.

CHAPTER V

CONCLUSIONS

The range of accuracy of the experimental measurements of this thesis is not exactly known. It is recognized that the electromagnetic-analogy method used has certain inherent inaccuracies. However, the greatest sources of error are probably the assumptions that the wake of a hovering rotor is a uniform vortex cylinder, that the sheet strength of the cylinder is constant along the wake, and that the relation between the thrust and the sheet strength is only slightly affected by the presence of the ground plane. In the real case, the wake spreads out along the ground, somewhat as shown in Figure 12. Also, the sheet strength is known to be a function of the distance from the rotor plane, as measured along the wake. Other sources of error include :

1. Variations in primary coil current
2. Errors in positioning the search coil
3. Meter reading errors
4. Distortion of the magnetic field about the model due to the labratory structure
5. Errors in plotting and drawing the graphs

The comparison between the experimental results and the mathematical results of reference 1 indicates that the experimental results should be sufficiently accurate for engineering purposes within the limits of the approximations made.

Values of V_i/v contained in Table 1 and Figure 5, together with values of V_i/v calculated by the method shown in Appendix II, provide the necessary information for computing the interference induced velocities for multi-rotor helicopters hovering in ground effect. A method for carrying out these computations is illustrated in the sample problem of Chapter IV.

APPENDIX

APPENDIX I

CALCULATION OF NONDIMENSIONAL NORMAL COMPONENT OF INDUCED VELOCITY AT THE NORMALIZING POINTS

The determination of the exact values of V_i/v at the normalizing points was accomplished by using the Biot-Savart relation which yields the relation shown in equation (3) of reference 1 :

$$V_i/v = (2)\ (\ell)\ \left[\frac{1}{\sqrt{\ell^2 + 1}} - \frac{1}{\sqrt{4\ \ell^2 + 1}}\right]$$

where $\ell = Z/R$

Therefore, for $Z/R = 0.5$,

$$V_i/v = (2)\ (\tfrac{1}{2})\ \left[\frac{1}{\sqrt{(\tfrac{1}{2})^2 + 1}} - \frac{1}{\sqrt{4\ (\tfrac{1}{2})^2 + 1}}\right] = 0.1874$$

The values for V_i/v at $Z/R = 1.0$, 1.5, and 2.0 were found in the same manner. These values of V_i/v are shown to three significant figures in the appropriate places in Table 1 (where $h/R = 0$ and $r/R = 0$). They are also shown to four significant figures in the table below.

Z/R	V_i/v
0.5	0.1874
1.0	0.5198
1.5	0.7154
2.0	0.8188

APPENDIX II

MATHEMATICAL METHOD OF CALCULATING NONDIMENSIONAL NORMAL COMPONENT OF INDUCED VELOCITY BY USING UNIFORM DISTRIBUTIONS OF SOURCES AND SINKS OVER CIRCULAR DISCS

Küchmann and Weber (3) showed that the flow field of a uniform distribution of sources or sinks over a circular disc is exactly equivalent to that of a semi-infinite vortex cylinder of constant strength providing the base of the cylinder and the disc coincide. The vortex cylinder is equivalent to the sum of doublet discs representing the individual vortex rings of the cylinder, the source and sink flows of which balance out, leaving only an equivalent distribution of sources or sinks on the initial surface at the end of the cylinder, and a corresponding distribution of sinks or sources, respectively, at infinity. The equivalence of the uniform distribution of sources or sinks to the uniform cylinder is valid only for points outside the limits of the cylinder. For a point that is physically located within the limits of a given cylinder, several uniform distributions of sources and sinks may be superpositioned in such a manner that the point in question (and an infinitesimal increment ϵ above and below the point) effectively lies outside the limits of the cylinders.

As mentioned in the sample problem of Chapter IV, there were seven points in the plane of the front rotor which were in or near the region of overlap between the front and rear rotors, and for which no experimental values of V_i/v were available. The points in question in

or near the overlap region were located such that with respect to the front rotor, $\psi = 0^\circ$, $r/R = 0.4$, 0.6, 0.8, and 1.0, and $\psi = 315^\circ$, $r/R = 0.6$, 0.8, and 1.0.

The superposition of six uniform distributions of sources and sinks as shown in Figure 13 would make it possible to effectively place all seven of the sample points in question outside the limits of the uniform wake vortex cylinder of the rear rotor. Utilizing this superposition, the nondimensional normal component of induced velocity could then be found at a number of points for which $h/R = -0.2$, $r/R < 1.2$, the range of values including the positions of the seven sample points. The manner in which the superposition shown in Figure 13 was actually accomplished is shown diagramatically in Figure 14. First, a uniform distribution of sinks was placed over a circular disc at q, the flow field of which is equivalent to the vortex cylinder shown in Figure 14 (a). Then, as shown in Figure 14 (b), a uniform distribution of sources was placed at r. The superposition of these two distributions produced the finite length vortex cylinder of Figure 14 (c). In a similar manner, placing a uniform distribution of sinks at s (an infinitesimal distance ϵ below r), and sources at t, resulted in another finite length vortex cylinder as shown in Figures 14 (d) - (f). In the image system, the superposition of a uniform distribution of sources at u (an infinitesimal distance ϵ below t), and sinks at v, yielded another finite length vortex cylinder as shown in Figures 14 (g) - (i). The superposition, then, of the velocities induced by these six uniform distributions of sources and sinks is equivalent to the sum of the velocities induced for the six superimposed semi-infinite vortex cylinders shown in Fig-

ure 14. The effect of the six semi-infinite vortex cylinders is also equivalent to that of the three finite length vortex cylinders shown in Figures 14 (j) or 13. It can be seen from these last two figures that a typical point P in the plane of the front rotor (h/R = - 0.2) is effectively outside the limits of the wake vortex cylinders.

Table 15 of the Appendix to reference 3 contains values of $\pi (V_i/v)$ for points in the vicinity of a uniform distribution of sources over a circular disc (or correspondingly, in the vicinity of a semi-infinite uniform vortex cylinder), for values of r/R and x/R equal to or less than two. If values of $\pi (V_i/v)$ are desired for r/R > 2 or x/R > 2, they may be calculated by the formulas given in reference 3. For a sink distribution, the signs of the tabular values are simply reversed. Data from this table were used to find the nondimensional normal component of velocity induced by the rear rotor (where Z/R = 1.0) at a number of points in the plane of the front rotor in and near the overlap region. An example of how the values at these points were calculated is shown below for a point located such that, with respect to the rear rotor, h/R = - 0.2 and r/R = 0.6 (see Figure 13). The value of $\pi(V_i/v)$ produced by each distribution of sources or sinks is shown individually, a positive sign indicating a downflow.

	x/R	$\pi (V_i/v)$
uniform distribution of sinks at q	0.2	- 2.31
uniform distribution of sources at r	0.0	+ 3.14
uniform distribution of sinks at s	0.0	+ 3.14
uniform distribution of sources at t	0.8	- 0.98
uniform distribution of sources at u	0.8	- 0.98
uniform distribution of sinks at v	1.8	+ 0.36
	Total	+ 2.37

Therefore, $V_i/v = \frac{\pm 2.37}{\pi} = + 0.755$

The values of V_i/v for other points were similarly calculated and the results presented in Figure 10 and Table 2. The locations of these points included the region containing the seven sample points mentioned above.

In order to compare the results of the two methods, the method of uniform distributions of sources and sinks was used to compute V_i/v at a number of points for which V_i/v was also obtained experimentally. The results agreed generally within $\pm$ 0.01 for points inside the wake vortex cylinder ($r/R < 1$), and within $\pm$ 0.03 for points in the region just outside the wake ($r/R > 1$). The close agreement of the two methods may be seen from Figure 10 if the curve for $Z/R = 1.0$, $h/R = - 0.2$ is examined. On this curve, at $r/R = 1.1$ and $r/R = 1.2$, the values of V_i/v were found using both methods.

TABLE 1. Measured Values of the Nondimensional Normal Component of Induced Velocity Along the Radius For a Rotor With Uniform Loading Obtained by Electromagnetic-analog

(a) For Nondimensional Ground Distance Z/R = 0.5

r/R	V_i/v for values of h/R of -								
	0	0.05	0.10	0.20	0.30	-0.05	-0.10	-0.20	-0.30
0.0	.187	.190	.188	.182	.170	.180	.175	-	-
0.2	.196	.196	.196	.187	.172	.190	.187	-	-
0.4	.238	.231	.223	.199	.179	.230	.230	-	-
0.6	.320	.298	.272	.221	.181	.326	.336	-	-
0.8	.458	.386	.315	.204	.153	.514	.565	-	-
0.9	.554	.395	.271	.159	.114	.666	.721	-	-
0.95	-	.326	.201	.119	.090	-	-	-	-
1.00	-	.090	.076	.069	.057	-	-	-	-
1.05	-	-.108	-.020	.023	.034	-	-	-	-
1.10	-.312	-.187	-.096	-.019	.006	-.468	-.502	-.534	-.501
1.15	-	-.188	-	-.044	-.010	-.359	-.405	-.434	-.401
1.2	-.236	-.177	-.130	-.060	-.023	-.288	-.329	-.346	-.304
1.4	-	-.113	-	-	-	-.138	-.145	-.141	-.111
1.6	-.067	-.064	-.059	-.051	-.040	-.068	-.070	-.064	-.049
1.8	-	-.038	-	-.026	-	-.038	-.037	-.031	-.022
2.0	-.022	-.022	-.022	-.021	-.020	-.021	-.020	-.017	-.012
2.4	-.009	-.009	-.009	-.009	-.010	-.008	-.008	-.006	-.004
2.8	-.004	-.004	-.004	-.005	-.005	-.004	-.003	-.003	-.002
3.2	-.002	-.002	-.002	-.002	-.003	-.002	-.002	-.001	-.001
3.6	-.001	-.001	-.001	-.001	-.001	-.001	-.001	-.001	0
4.0	-.001	-.001	-.001	-.001	-.001	-.001	-.001	0	0
4.4	0	0	0	0	-.001	0	0	0	0
4.8	0	0	0	0	0	0	0	0	0
5.2	0	0	0	0	0	0	0	0	0
5.6	0	0	0	0	0	0	0	0	0
6.0	0	0	0	0	0	0	0	0	0

TABLE 1. Continued

(b) For Nondimensional Ground Distance Z/R = 1.0

r/R	V_i/v for values of h/R of -								
	0	0.05	0.10	0.20	0.30	-0.05	-0.10	-0.20	-0.30
0.0	.520	.499	.476	.435	.381	-	-	-	-
0.2	.523	.507	.484	.439	.383	-	-	-	-
0.4	.544	.527	.498	.440	.375	-	-	-	-
0.6	.594	.552	.517	.430	.351	-	-	-	-
0.8	.668	.582	.500	.366	.282	-	-	-	-
0.9	.726	.540	.423	.284	.217	-	-	-	-
0.95	-	.463	.328	.226	.176	-	-	-	-
1.00	-	.180	.172	.149	.133	-	-	-	-
1.05	-	-.036	.038	.091	.099	-	-	-	-
1.10	-.273	-.141	-.051	.034	.057	-	-.455	-.497*	-.538
1.15	-.243	-.157	-.090	-.003	.031	-	-.381	-.432*	-.483
1.20	-.226	-.162	-.111	-.034	.008	-	-.330	-.378*	-.426
1.4	-.159	-.138	-.117	-.077	-.044	-	-.200	-.228*	-.256
1.6	-.116	-.105	-.094	-.072	-.053	-	-.135	-.147*	-.160
1.8	-.082	-.076	-.072	-.059	-.048	-	-.090	-.096*	-.102
2.0	-.057	-.055	-.052	-.047	-.040	-	-.061	-.063*	-.065
2.4	-.031	-.030	-.030	-.028	-.025	-	-.031	-.031*	-.031
2.8	-.017	-.017	-.016	-.016	-.015	-	-.016	-.015*	-.015
3.2	-.010	-.010	-.010	-.010	-.010	-	-.009	-.008*	-.008
3.6	-.006	-.006	-.006	-.006	-.006	-	-.005	-.005*	-.005
4.0	-.004	-.004	-.004	-.004	-.004	-	-.003	-.003*	-.003
4.4	-.002	-.002	-.002	-.002	-.003	-	-.002	-.002*	-.002
4.8	-.001	-.002	-.002	-.002	-.002	-	-.001	-.001*	-.001
5.2	-.001	-.001	-.001	-.001	-.001	-	-.001	-.001*	-.001
5.6	-.001	-.001	-.001	-.001	-.001	-	-.001	-.001*	-.001
6.0	-.001	-.001	-.001	-.001	-.001	-	0	0*	0

* - Values obtained by linear interpolation

TABLE 1. Continued

(c) For Nondimensional Ground Distance Z/R = 1.5

r/R	V_i/v for values of h/R of -								
	0	0.05	0.10	0.20	0.30	-0.05	-0.10	-0.20	-0.30
0.0	.715	.682	.645	.568	.509	-	-	-	-
0.2	.720	.685	.652	.568	.504	-	-	-	-
0.4	.735	.694	.652	.559	.487	-	-	-	-
0.6	.753	.706	.645	.534	.449	-	-	-	-
0.8	.786	.699	.602	.450	.359	-	-	-	-
0.9	.816	.645	.512	.357	.280	-	-	-	-
0.95	-	.533	.402	.291	.237	-	-	-	-
1.00	-	.260	.237	.211	.190	-	-	-	-
1.05	-	.025	.106	.147	.146	-	-	-	-
1.10	-.204	-.077	.003	.081	.106	-	-.388	-.432*	-.477
1.15	-.183	-.101	-.035	.044	.076	-	-.327	-.379*	-.431
1.20	-.172	-.115	-.063	.010	.049	-	-.282	-.331*	-.381
1.4	-.138	-.115	-.093	-.051	-.020	-	-.184	-.219*	-.254
1.6	-.112	-.099	-.086	-.062	-.043	-	-.137	-.157*	-.178
1.8	-.088	-.080	-.074	-.059	-.046	-	-.103	-.117*	-.130
2.0	-.071	-.067	-.062	-.052	-.043	-	-.079	-.087*	-.095
2.4	-.045	-.043	-.041	-.037	-.033	-	-.048	-.050*	-.053
2.8	-.028	-.027	-.027	-.025	-.023	-	-.029	-.030*	-.032
3.2	-.018	-.018	-.018	-.017	-.016	-	-.019	-.019*	-.019
3.6	-.012	-.012	-.012	-.012	-.011	-	-.012	-.012*	-.012
4.0	-.008	-.008	-.008	-.008	-.008	-	-.008	-.008*	-.008
4.4	-.005	-.005	-.005	-.005	-.005	-	-.005	-.005*	-.005
4.8	-.004	-.004	-.004	-.004	-.004	-	-.004	-.003*	-.003
5.2	-.003	-.003	-.003	-.003	-.003	-	-.002	-.002*	-.002
5.6	-.002	-.002	-.002	-.002	-.002	-	-.002	-.002*	-.002
6.0	-.001	-.001	-.001	-.001	-.001	-	-.001	-.001*	-.001

* - Values obtained by linear interpolation

TABLE 1. Continued

(d) For Nondimensional Ground Distance Z/R = 2.0

r/R	V_i/v for values of h/R of -								
	0	0.05	0.10	0.20	0.30	-0.05	-0.10	-0.20	-0.30
0.0	.819	.773	.738	.650	.573	-	-	-	-
0.2	.823	.777	.738	.650	.569	-	-	-	-
0.4	.829	.778	.735	.636	.550	-	-	-	-
0.6	.842	.780	.721	.603	.505	-	-	-	-
0.8	.861	.759	.665	.511	.408	-	-	-	-
0.9	.881	.708	.569	.415	.332	-	-	-	-
0.95	-	.617	.482	.357	.287	-	-	-	-
1.00	-	.349	.320	.265	.236	-	-	-	-
1.05	-	.101	.174	.196	.195	-	-	-	-
1.10	-.165	-.025	.063	.132	.146	-.308	-.349	-.410	-.422
1.15	-.144	-.057	.010	.083	.116	-.233	-.284	-.353	-.373
1.20	-.136	-.076	-.025	.050	.083	-.199	-.244	-.304	-.335
1.4	-.113	-.089	-.068	-.025	.005	-.136	-.158	-.197	-.227
1.6	-.094	-.081	-.071	-.047	-.025	-.108	-.120	-.146	-.166
1.8	-.081	-.072	-.065	-.049	-.035	-.088	-.095	-.113	-.126
2.0	-.069	-.062	-.058	-.047	-.037	-.074	-.078	-.088	-.097
2.4	-.049	-.045	-.043	-.038	-.033	-.051	-.053	-.058	-.062
2.8	-.034	-.033	-.031	-.028	-.026	-.035	-.036	-.039	-.041
3.2	-.024	-.023	-.022	-.021	-.020	-.024	-.025	-.026	-.027
3.6	-.017	-.017	-.016	-.016	-.015	-.017	-.018	-.018	-.018
4.0	-.012	-.012	-.012	-.011	-.011	-.012	-.012	-.013	-.013
4.4	-.008	-.008	-.008	-.008	-.008	-.009	-.008	-.009	-.009
4.8	-.006	-.006	-.006	-.006	-.006	-.006	-.006	-.006	-.006
5.2	-.005	-.005	-.005	-.005	-.005	-.005	-.005	-.005	-.004
5.6	-.004	-.003	-.003	-.003	-.003	-.003	-.004	-.003	-.003
6.0	-.003	-.003	-.003	-.003	-.003	-.003	-.003	-.003	-.002

TABLE 2. Calculated Values of the Nondimensional Normal Component of Induced Velocity Found by Using Uniform Distributions of Sources and Sinks Over Circular Discs

(1)	(2)	(3)	(4)	(5)	(6)	(7)	(8)	(9)
r/R	$(\pi V_i/v)_q$	$(\pi V_i/v)_r$	$(\pi V_i/v)_s$	$(\pi V_i/v)_t$	$(\pi V_i/v)_u$	$(\pi V_i/v)_v$	$(\pi V_i/v)$	(V_i/v)
0.0	3.14	0.0	0.0	-0.92	-0.92	0.33	1.63	0.518
0.2	-2.53	3.14	3.14	-1.15	-1.15	0.40	1.85	0.588
0.4	-2.46	3.14	3.14	-1.09	-1.09	0.39	2.03	0.646
0.5	-2.39	3.14	3.14	-1.04	-1.04	0.37	2.18	0.693
0.6	-2.31	3.14	3.14	-0.98	-0.98	0.36	2.37	0.755
0.8	-1.99	3.14	3.14	-0.84	-0.84	0.33	2.94	0.935
0.9	-1.69	3.14	3.14	-0.76	-0.76	0.31	3.38	1.075
0.95	-1.48	3.14	3.14	-0.71	-0.71	0.30	3.68	1.171
0.98	-1.34	3.14	3.14	-0.69	-0.69	0.30	3.86	1.226
1.00	-1.20	1.57	1.57	-0.67	-0.67	0.30	0.90	0.286
1.02	-1.10	0.0	0.0	-0.66	-0.66	0.29	-2.13	-0.678
1.05	-0.96	0.0	0.0	-0.63	-0.63	0.29	-1.93	-0.614
1.10	-0.74	0.0	0.0	-0.59	-0.59	0.28	-1.64	-0.522
1.20	-0.49	0.0	0.0	-0.52	-0.52	0.27	-1.26	-0.401

Column Explanation

(1) r/R measured from center of rear rotor whose Z/R = 1.0.

(2) $\pi (V_i/v)$ due to the uniform distribution of sinks at q, as shown in Figure 13.

(3) $\pi (V_i/v)$ due to the uniform distribution of sources at r, as shown in Figure 13.

(4) $\pi (V_i/v)$ due to the uniform distribution of sinks at s, as shown in Figure 13.

TABLE 2. Continued

(5) $\pi (V_i/v)$ due to the uniform distribution of sources at t, as shown in Figure 13.

(6) $\pi (V_i/v)$ due to the uniform distribution of sources at u, as shown in Figure 13.

(7) $\pi (V_i/v)$ due to the uniform distribution of sinks at v, as shown in Figure 13.

(8) $\pi (V_i/v)$ due to the superposition of uniform distributions of sources and sinks at q, r, s, t, u, and v.

(9) (V_i/v) = nondimensional normal component of induced velocity.

TABLE 3. Calculated Values of the Nondimensional Normal Component of Induced Velocity Along the Radius For Various Azimuth Angles for Z/R = 1.0, h/R = -0.2, and For Z/R = 0.8, h/R = + 0.2

(1)	(2)	(3)	(4)	(5)	(6)	(7)	(8)
ψ	r/R	P	P/R	V_i/v	Q	Q/R	V_i/v
0°	0.0	400.0	1.429	-0.080	400.0	1.429	-0.212
	0.2	456.0	1.629	-0.064	343.5	1.227	-0.350
	0.40	512.0	1.829	-0.046	288.0	1.029	-0.655*
	0.45	-	-	-	273.0	0.975	1.220*
	0.47	-	-	-	268.0	0.957	1.180*
	0.50	-	-	-	259.0	0.925	1.125*
	0.6	568.0	2.029	-0.036	232.0	0.829	0.970*
	0.8	624.0	2.229	-0.026	176.0	0.628	0.776*
	1.0	680.0	2.429	-0.020	120.0	0.428	0.659*
90°	0.2	403.5	1.441	-0.080	403.5	1.441	-0.207
	0.4	415.0	1.482	-0.076	415.0	1.482	-0.189
	0.6	433.5	1.548	-0.070	433.5	1.548	-0.164
	0.8	458.5	1.637	-0.064	458.5	1.638	-0.136
	1.0	488.0	1.743	-0.052	488.0	1.743	-0.109
135°	0.2	362.0	1.293	-0.068	441.5	1.577	-0.155
	0.4	330.0	1.179	-0.035	485.5	1.734	-0.110
	0.6	305.0	1.089	0.021	532.0	1.900	-0.080
	0.8	288.5	1.030	0.080	581.0	2.075	-0.058
	1.0	283.0	1.011	0.101	630.0	2.250	-0.040
180°	0.2	343.5	1.227	-0.051	456.0	1.629	-0.139
	0.4	288.0	1.029	0.082	512.0	1.829	-0.091
	0.6	232.0	0.829	0.290	568.0	2.029	-0.062
	0.8	176.0	0.629	0.351	624.0	2.229	-0.040
	1.0	120.0	0.428	0.355	680.0	2.429	-0.030

TABLE 3. Continued

(1)	(2)	(3)	(4)	(5)	(6)	(7)	(8)
ψ	r/R	P	P/R	V_i/v	Q	Q/R	V_i/v
270°	0.2	403.5	1.441	-0.080	403.5	1.441	-0.207
	0.4	415.0	1.482	-0.076	415.0	1.482	-0.189
	0.6	433.5	1.548	-0.070	433.5	1.548	-0.164
	0.8	458.5	1.637	-0.064	458.5	1.637	-0.136
	1.0	488.0	1.743	-0.052	488.0	1.743	-0.109
315°	0.2	441.5	1.577	-0.068	362.0	1.293	-0.297
	0.4	485.5	1.743	-0.052	330.0	1.179	-0.399
	0.6	532.0	1.900	-0.040	305.0	1.089	-0.541*
	0.8	581.0	2.075	-0.032	288.5	1.030	-0.655*
	1.0	630.0	2.250	-0.025	283.0	1.011	-0.685*

* - Values of V_i/v the calculation of which required use of the method of uniform distributions of sources and sinks over circular discs.

Column Explanation

(1) Azimuth angle measured from downwind position

(2) Nondimensional radius of points

(3) Distance in inches from center of front rotor to points in rear rotor

(4) Quantities in column (3) expressed nondimensionally

(5) V_i/v for points in the rear rotor which, with respect to the front rotor, are located at $h/R = +0.2$.

(6) Distance in inches from center of rear rotor to points in front rotor

(7) Quantities in column (6) expressed nondimensionally

(8) V_i/v for points in the front rotor which, with respect to the rear rotor, are located at $h/R = -0.2$

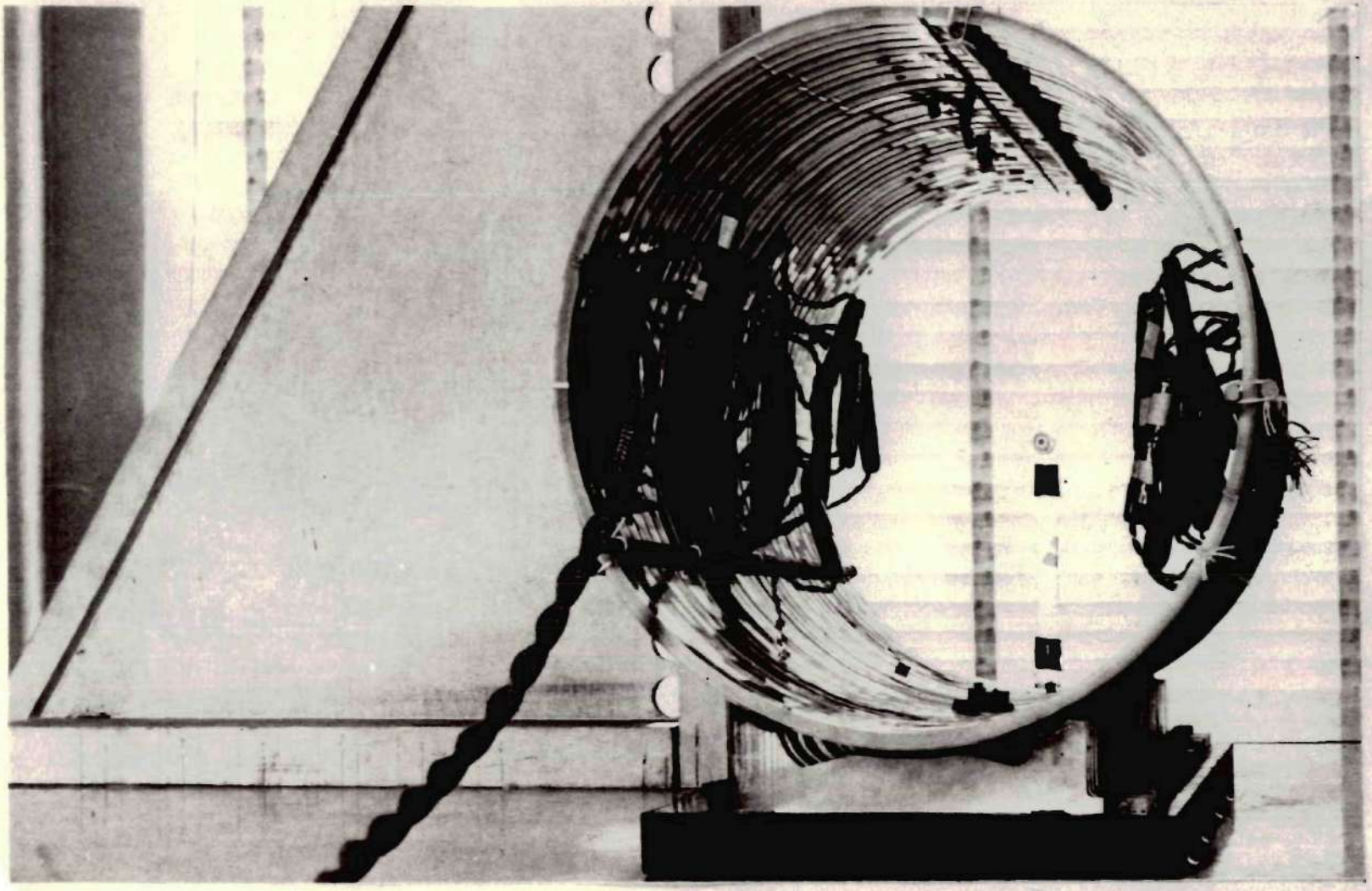

(a) View A

Figure 1. Electromagnetic-analogy Model Assembly

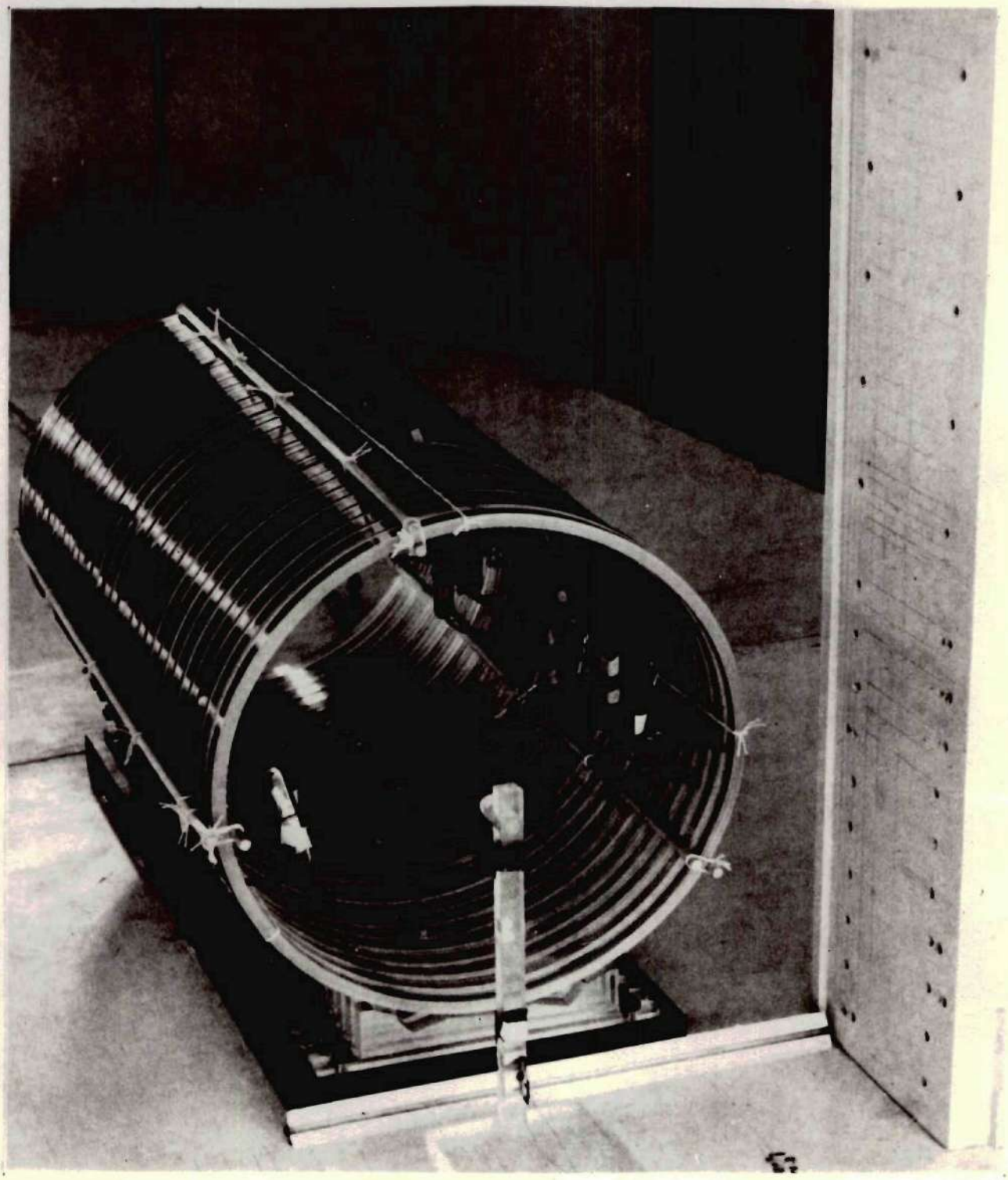

(b) View B

Figure 1. Continued

Figure 2. Search Coil Assembly

Figure 3. Fixed Frequency Amplifier and Indicator Unit

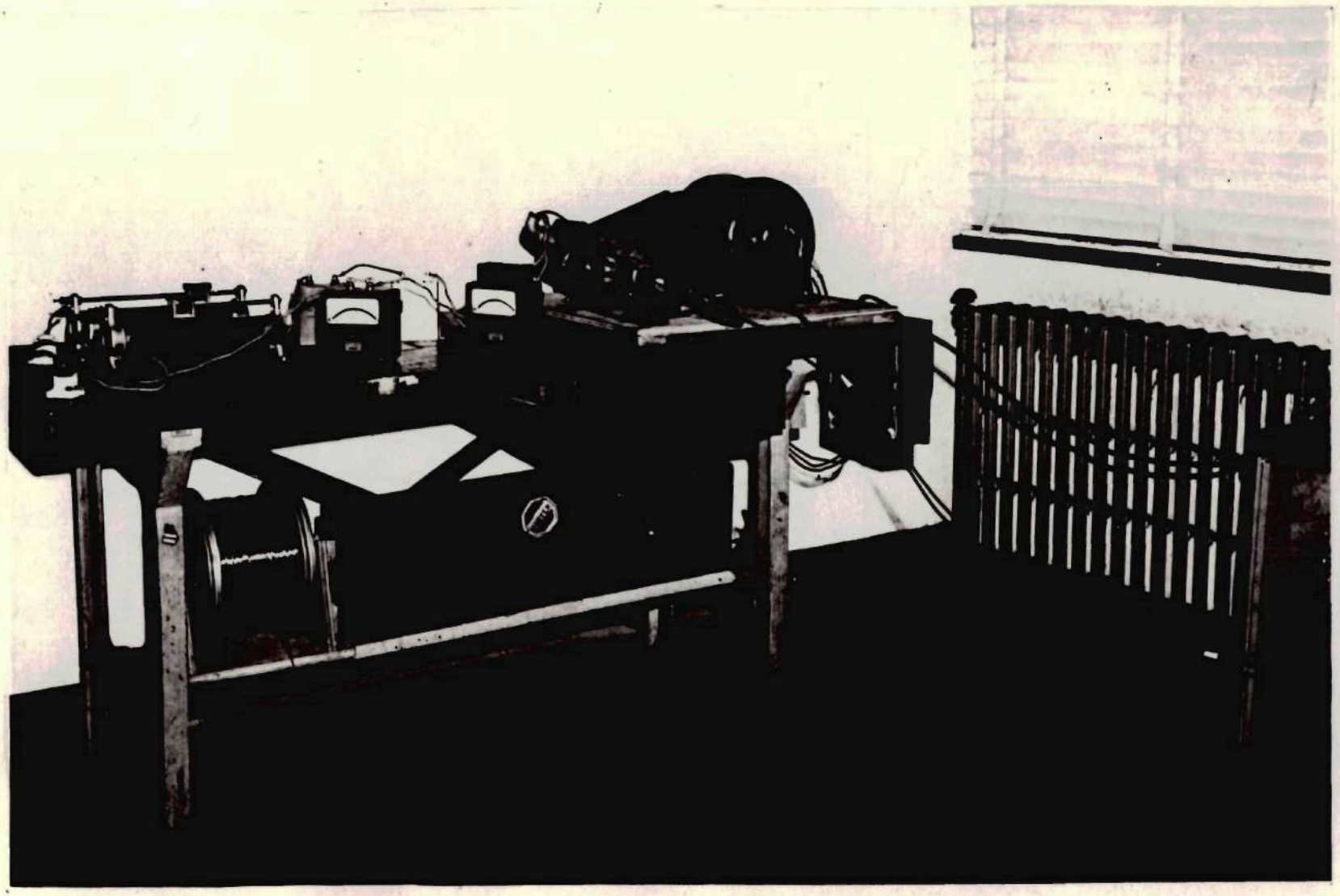

Figure 4. Power Supply Assembly

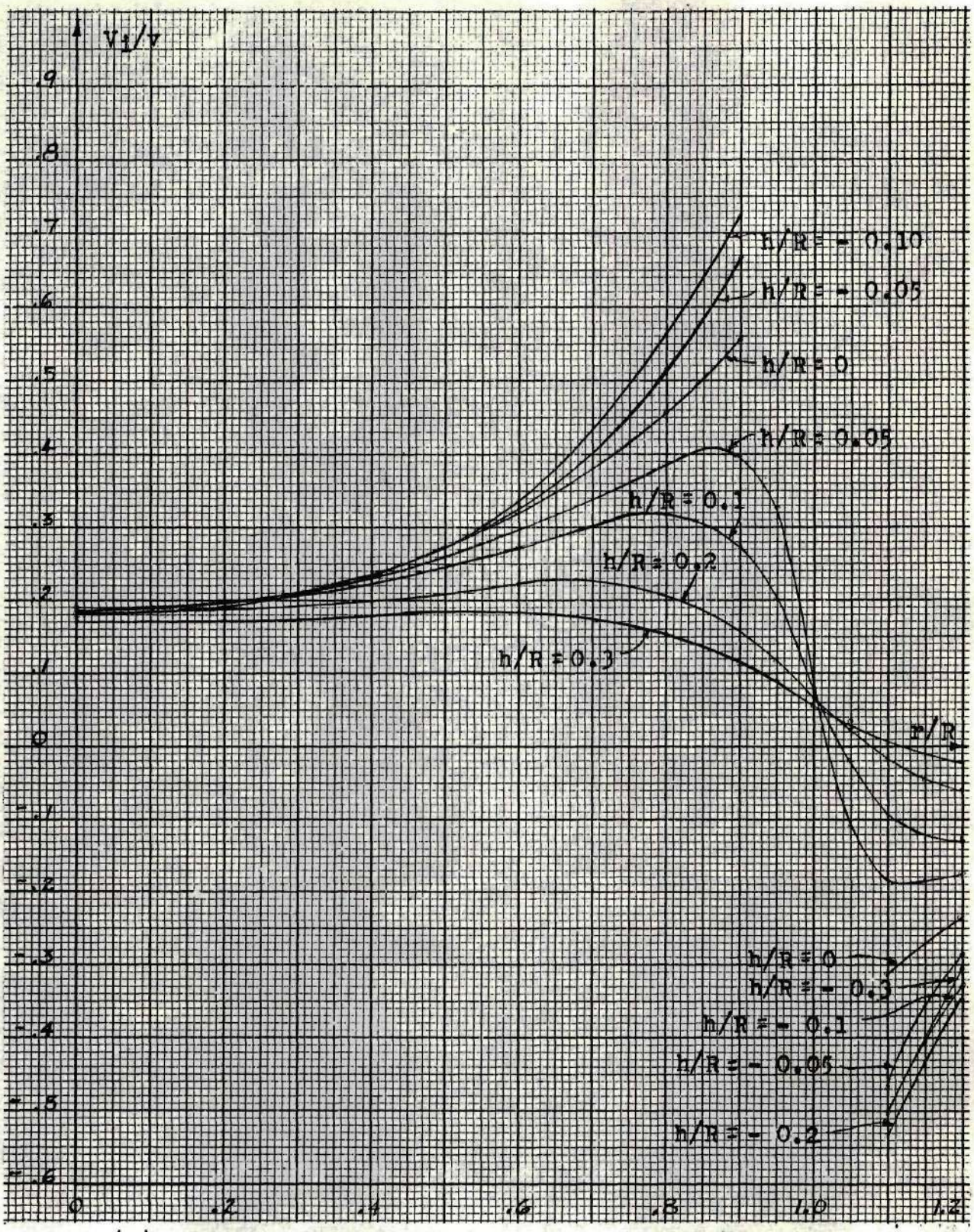

(a) For Nondimensional Ground Distance Z/R = 0.5

Figure 5. Variation of Nondimensional Normal Component of Induced Velocity Along the Radius For a Rotor With Uniform Loading

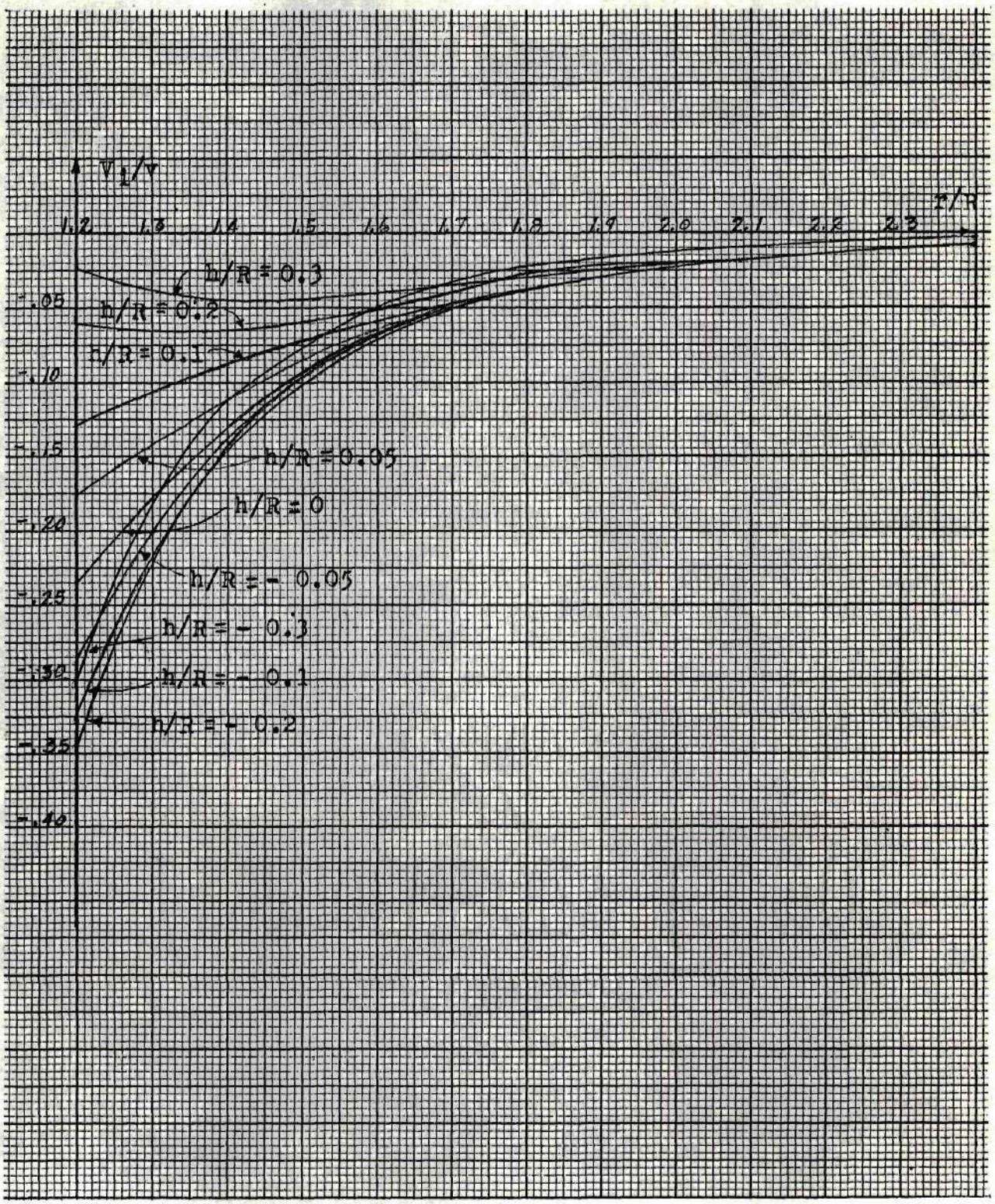

Figure 5(a). Continued

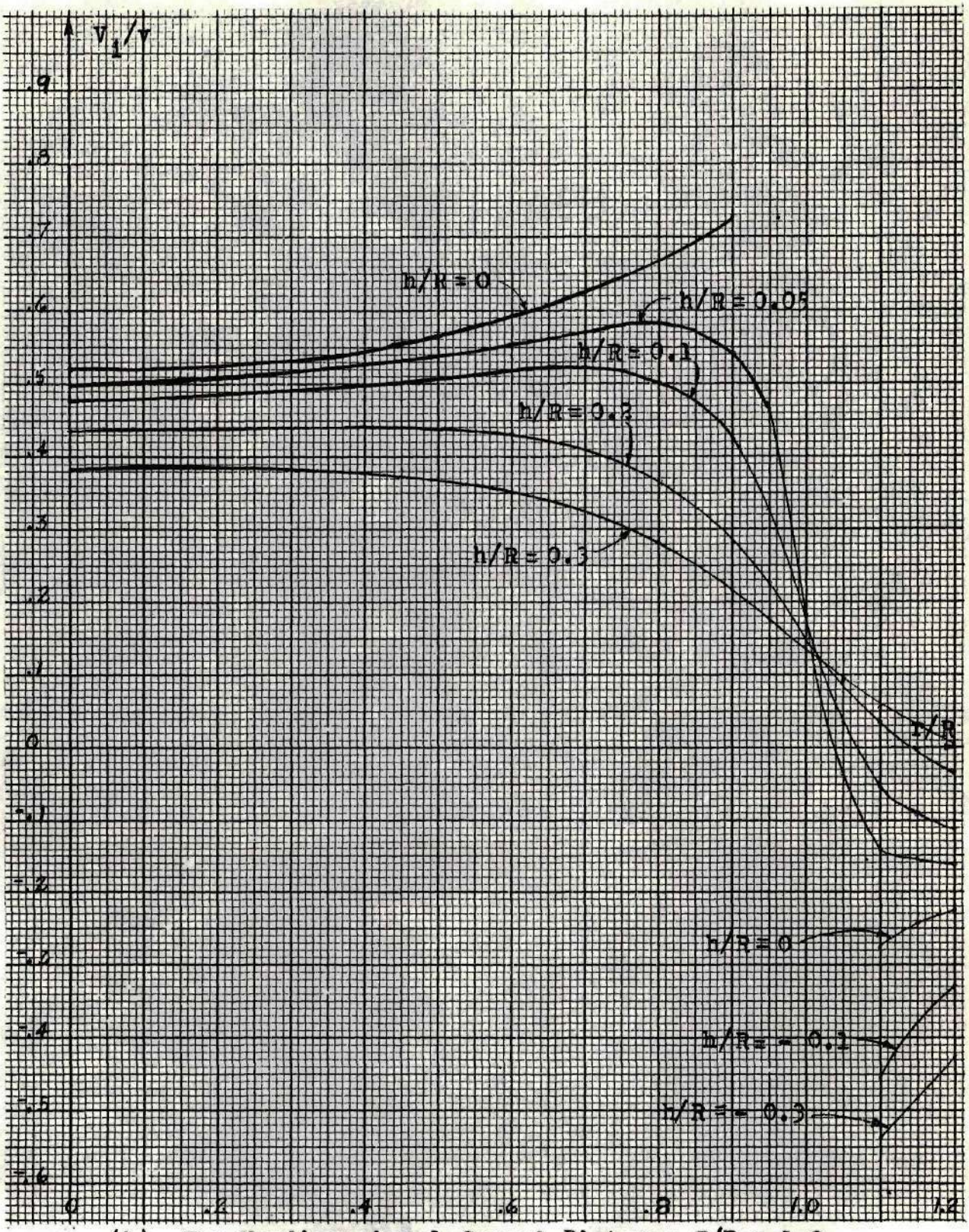

(b) For Nondimensional Ground Distance Z/R = 1.0

Figure 5. Continued

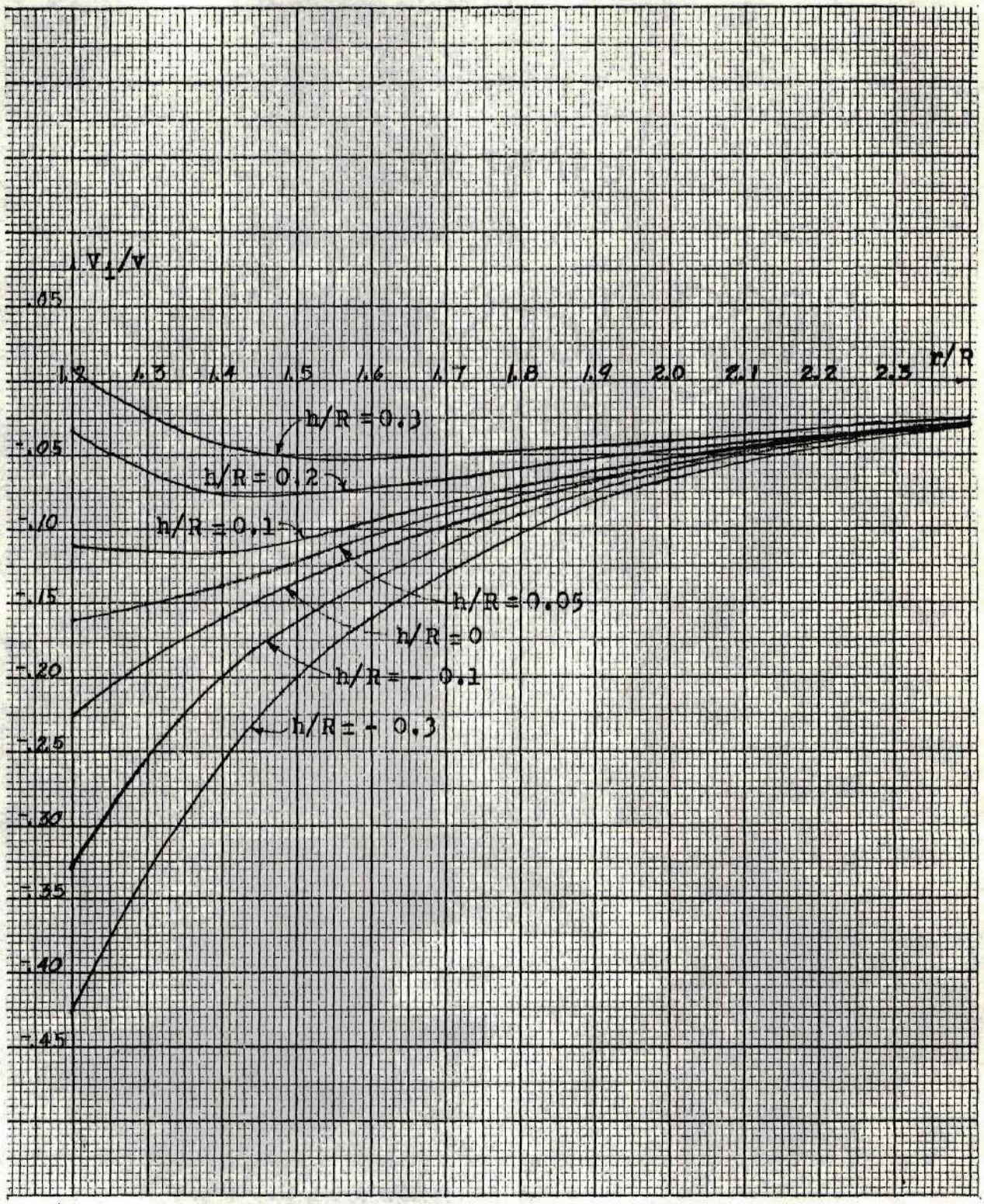

Figure 5(b). Continued

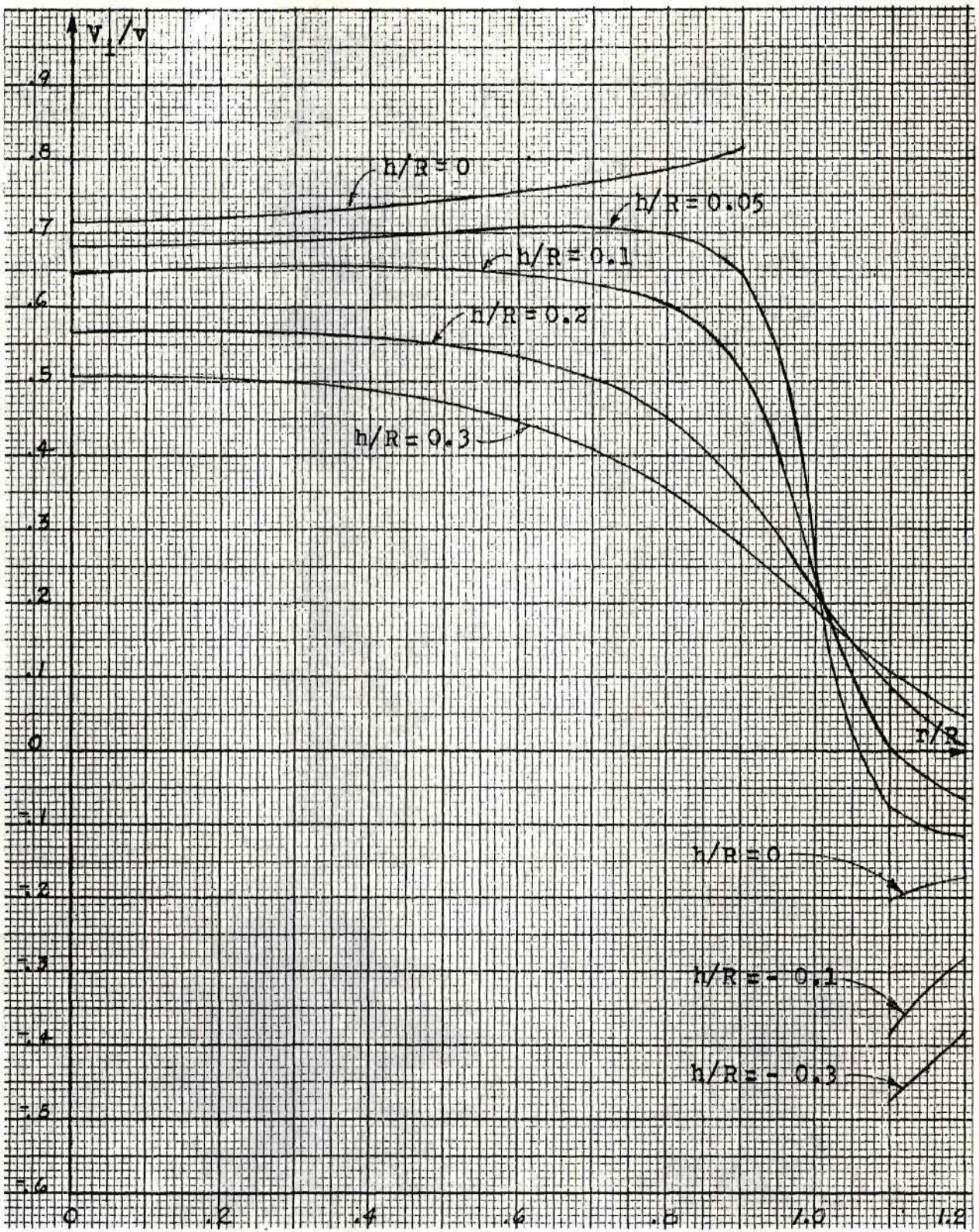

(c) For Nondimensional Ground Distance Z/R = 1.5

Figure 5. Continued

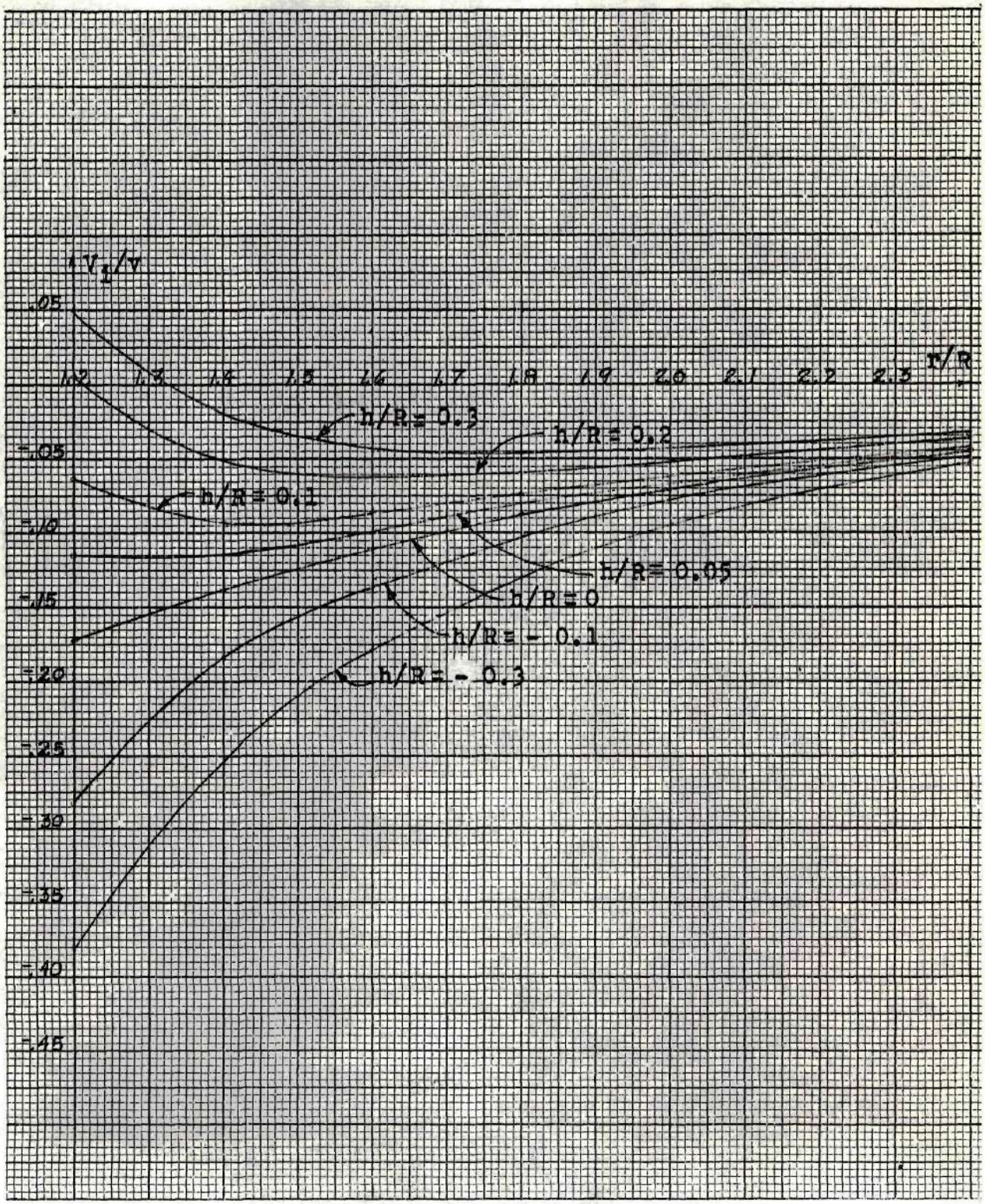

Figure 5(c). Continued

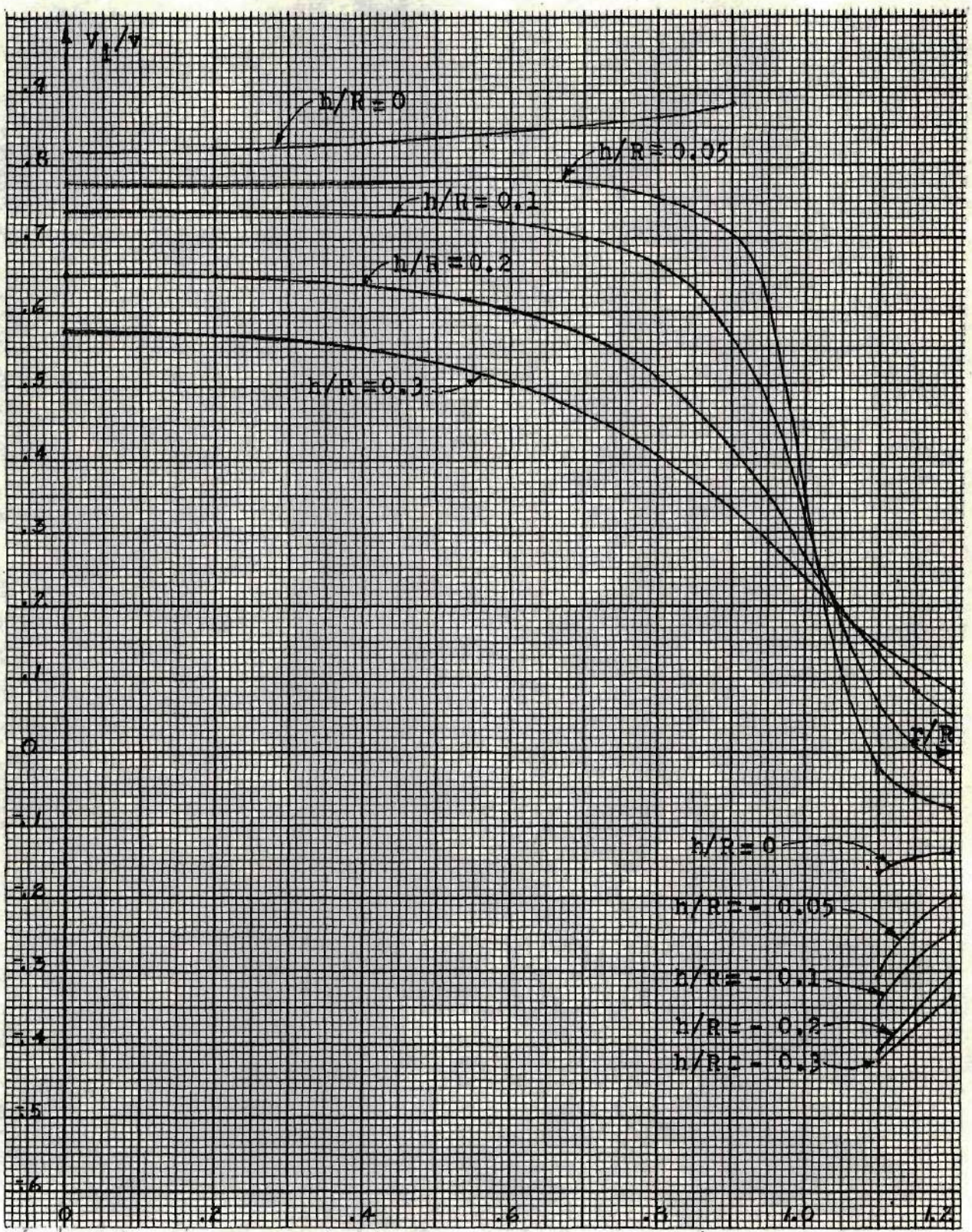

(d) For Nondimensional Ground Distance Z/R = 2.0

Figure 5. Continued

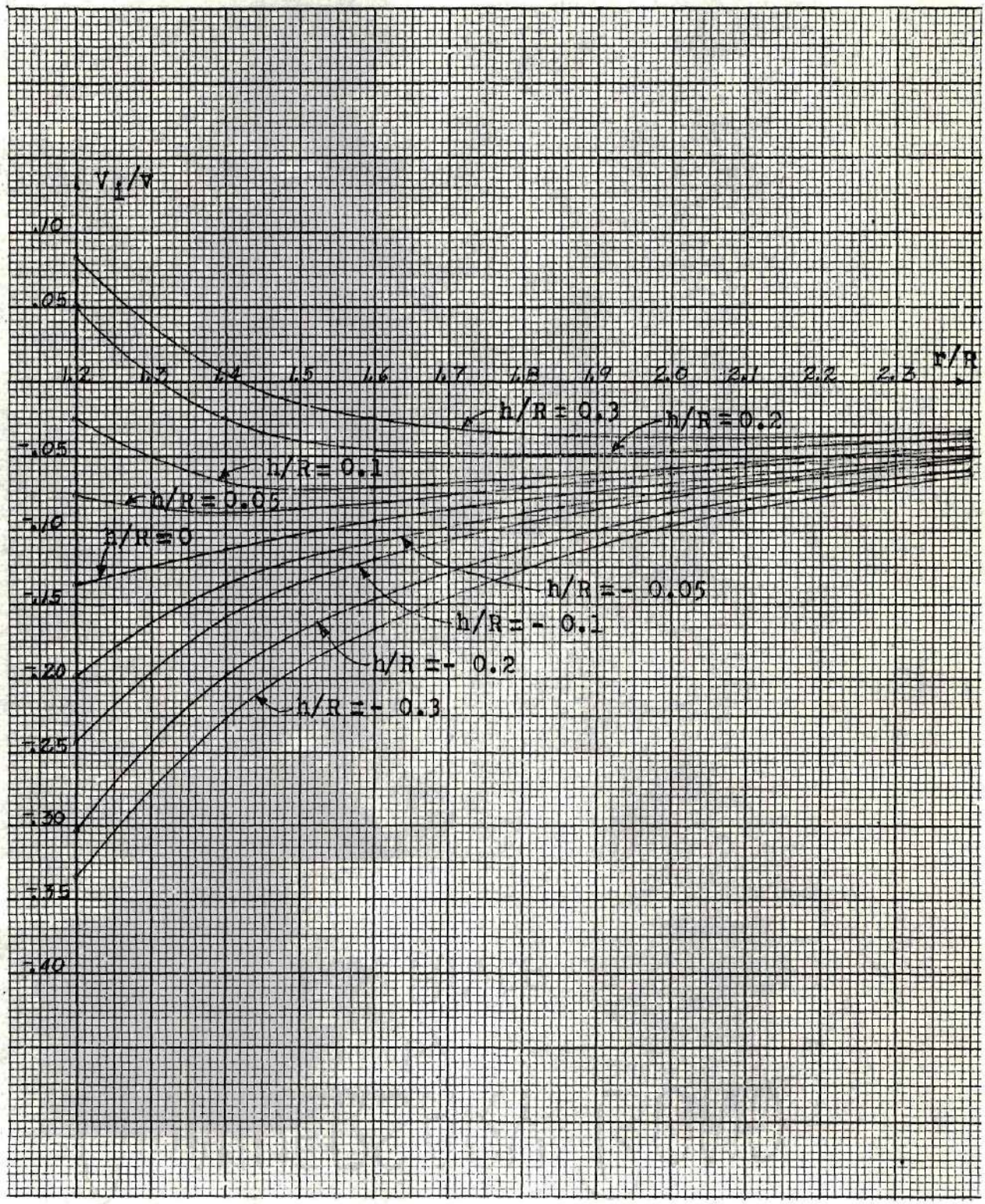

Figure 5(d). Continued

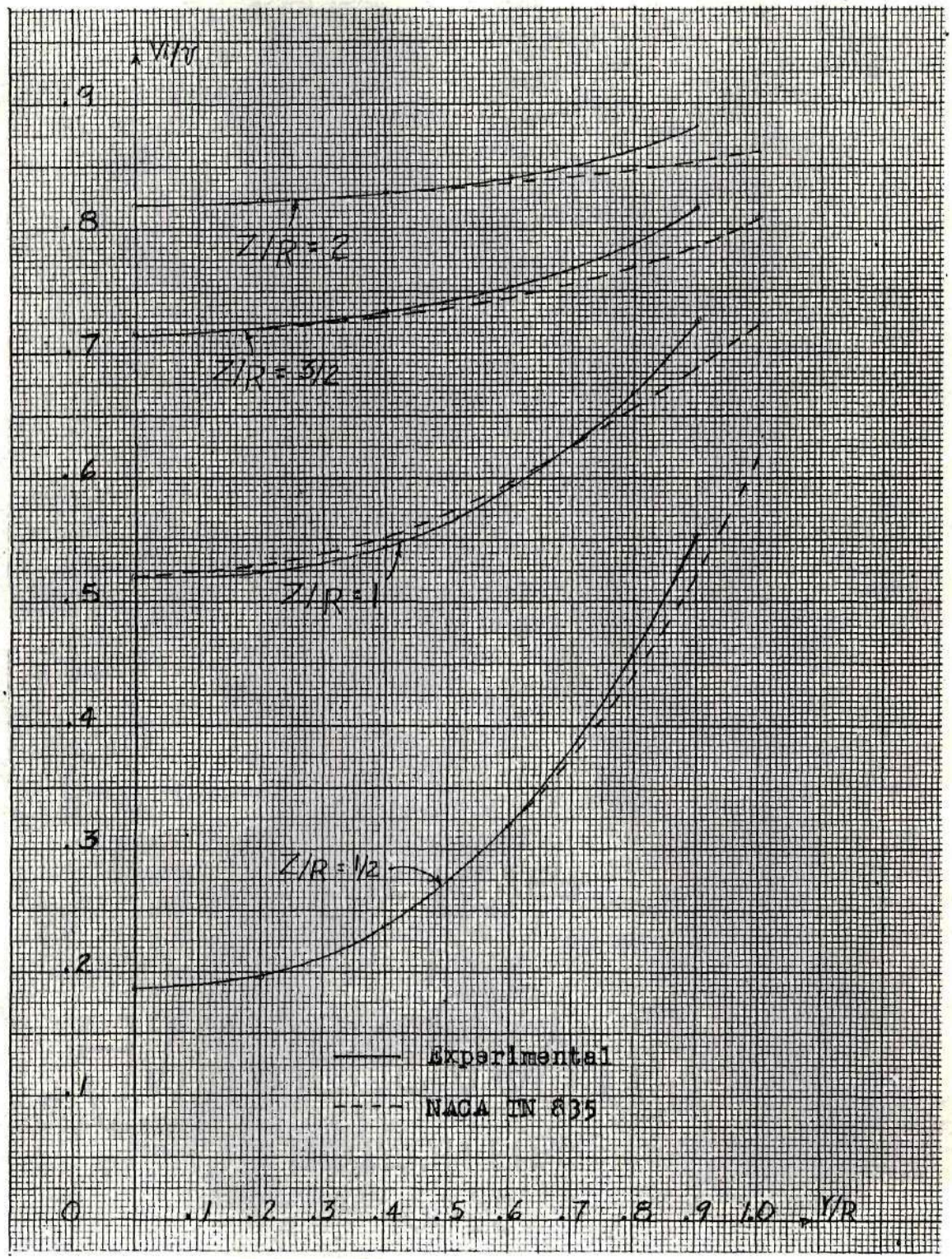

Figure 6. Comparison of Experimental Data With That From NACA TN 835

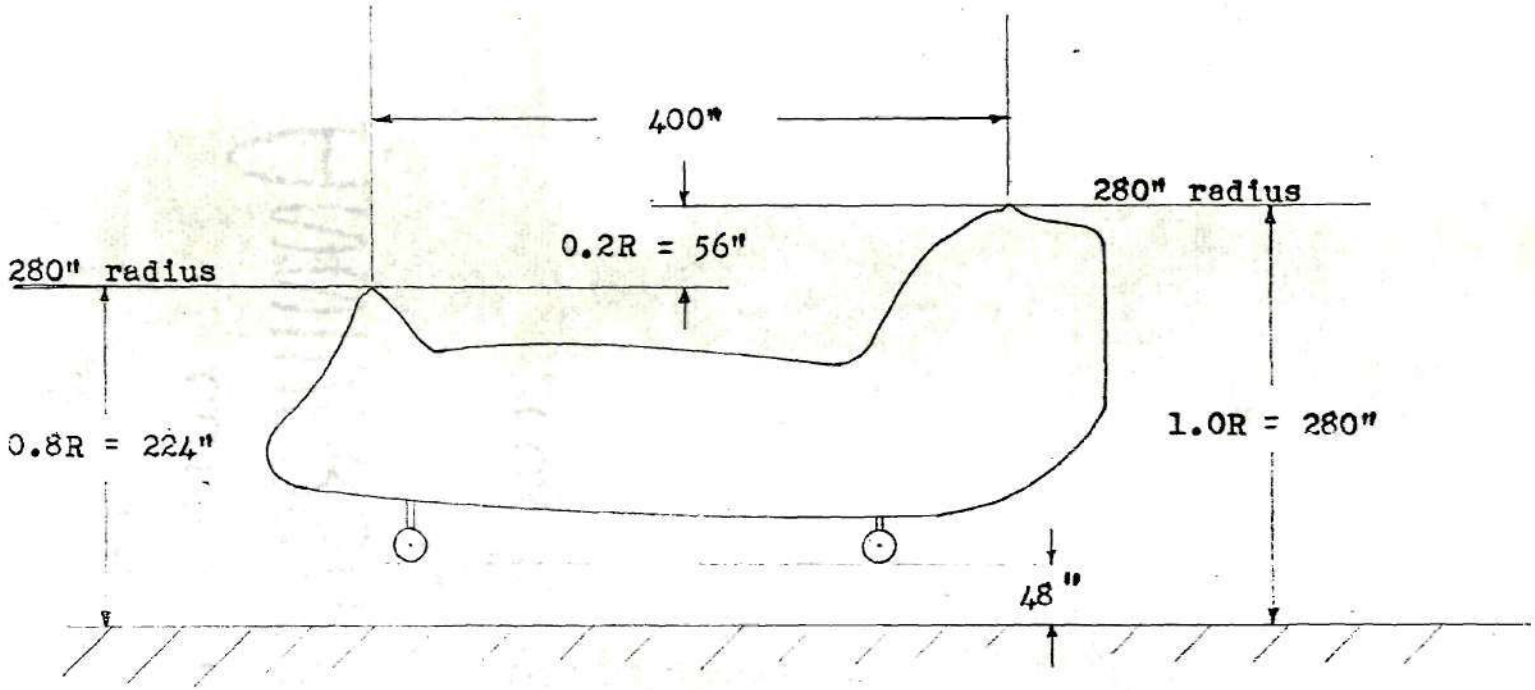

Figure 7. Dimensions and Configuration of Typical Tandem-rotor Helicopter Used in Sample Problem

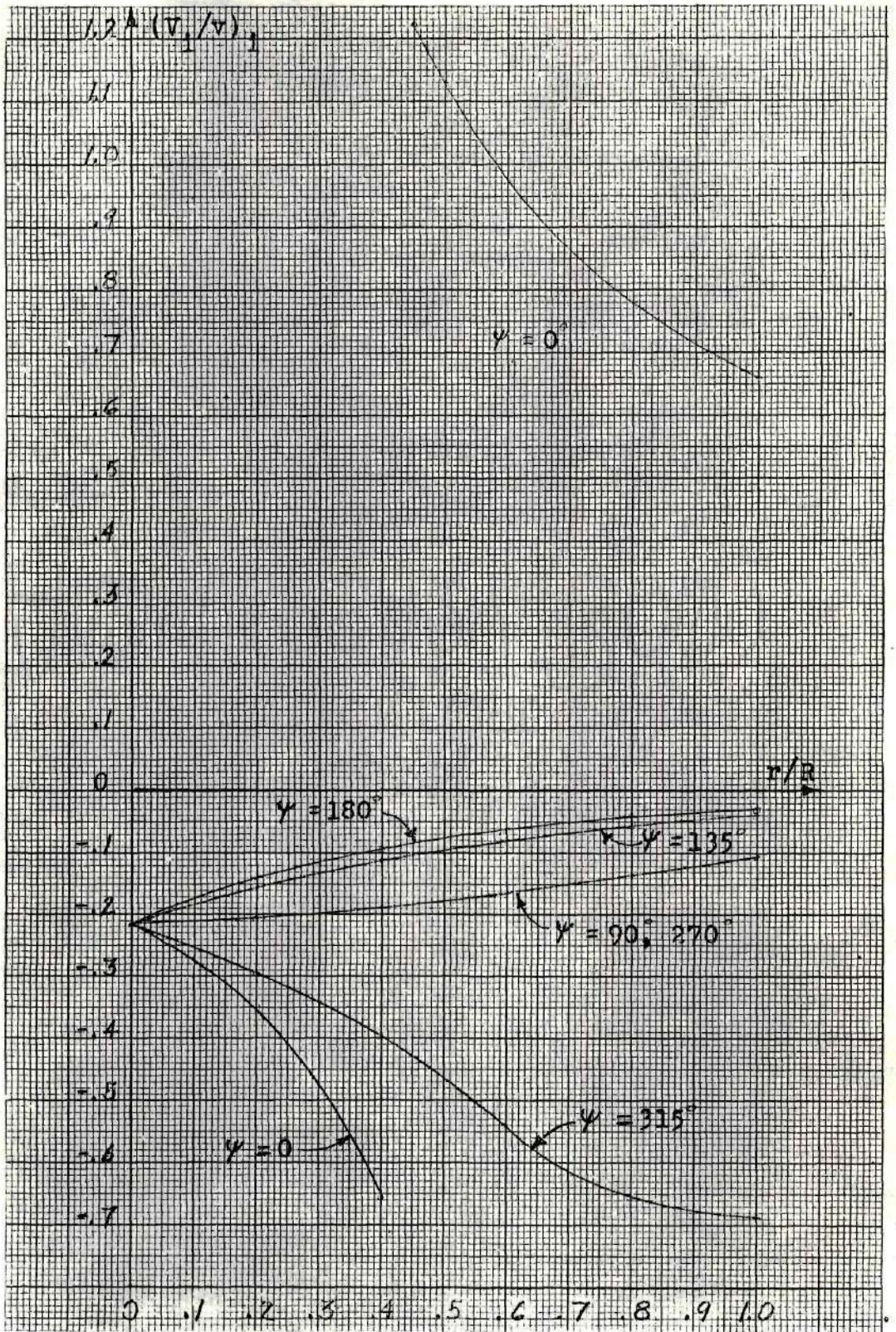

(a) For Front Rotor of Configuration Shown in Figure 7

Figure 8. Variation of Nondimensional Interference Induced Velocity Along the Radius For Various Azimuth Angles

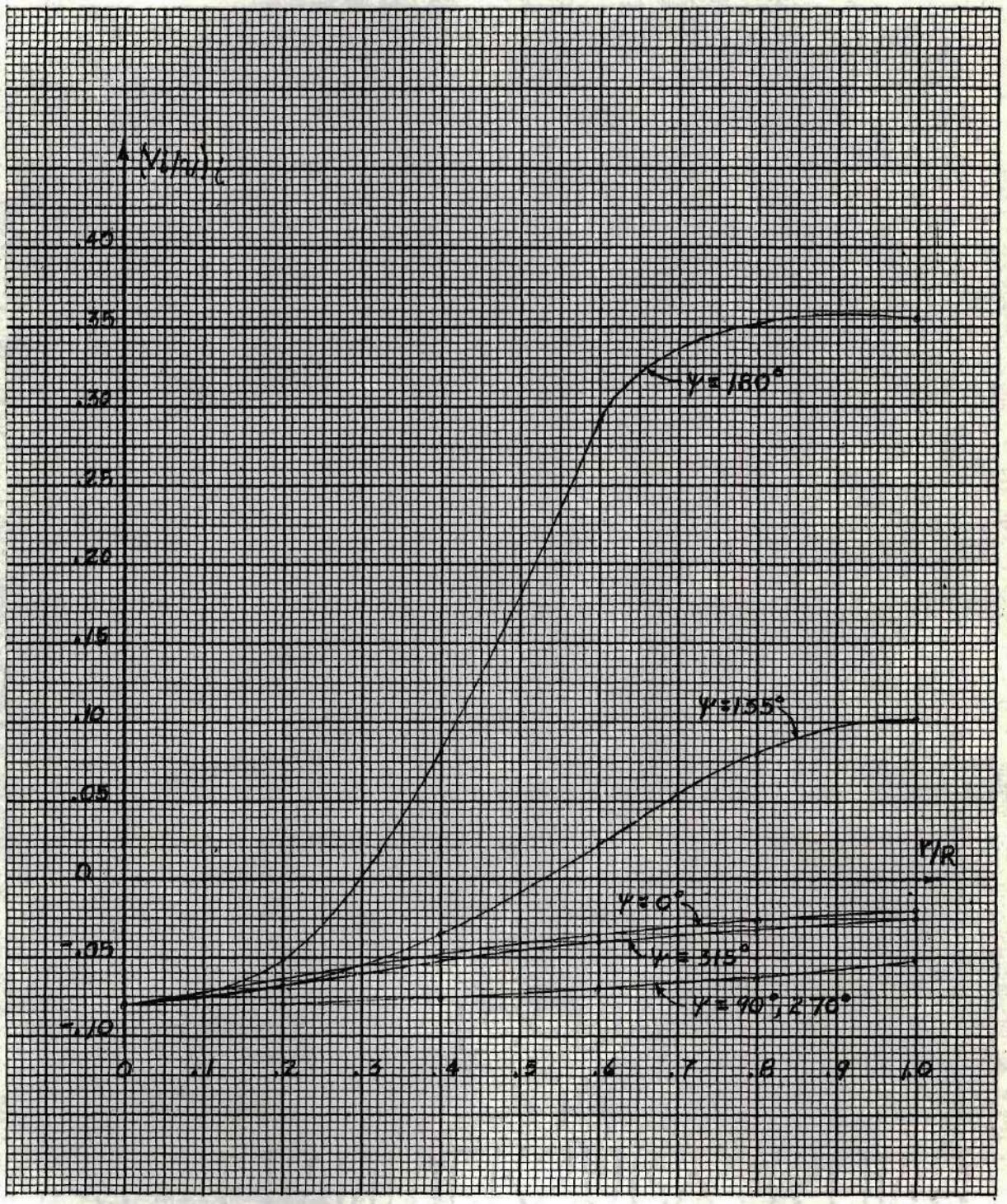

(b) For Rear Rotor of Configuration Shown in Figure 7.

Figure 8. Continued

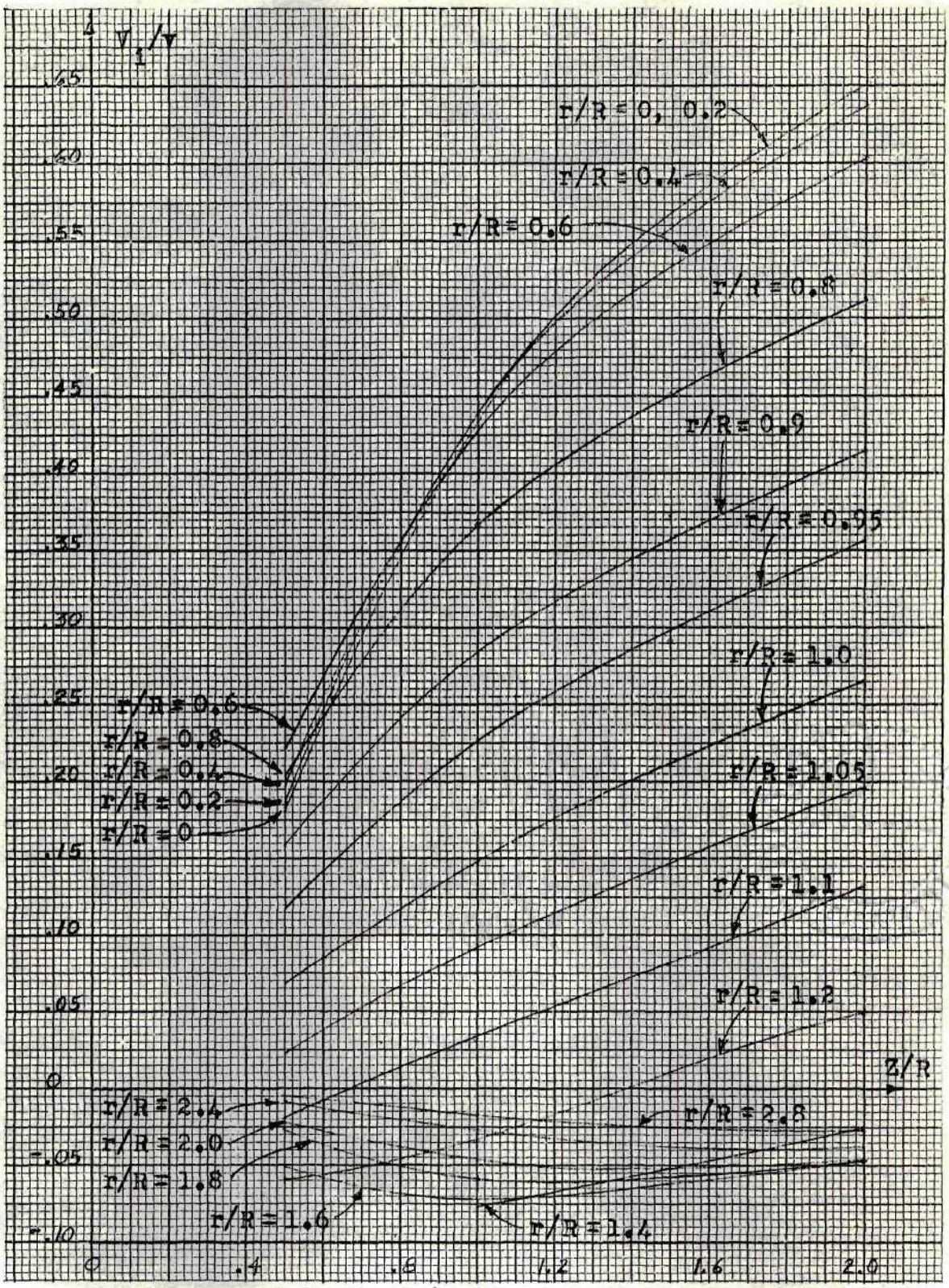

(a) For h/R = +0.2

Figure 9. Variation of Nondimensional Normal Component of Induced Velocity At Constant Radius For Different Nondimensional Ground Heights, Z/R

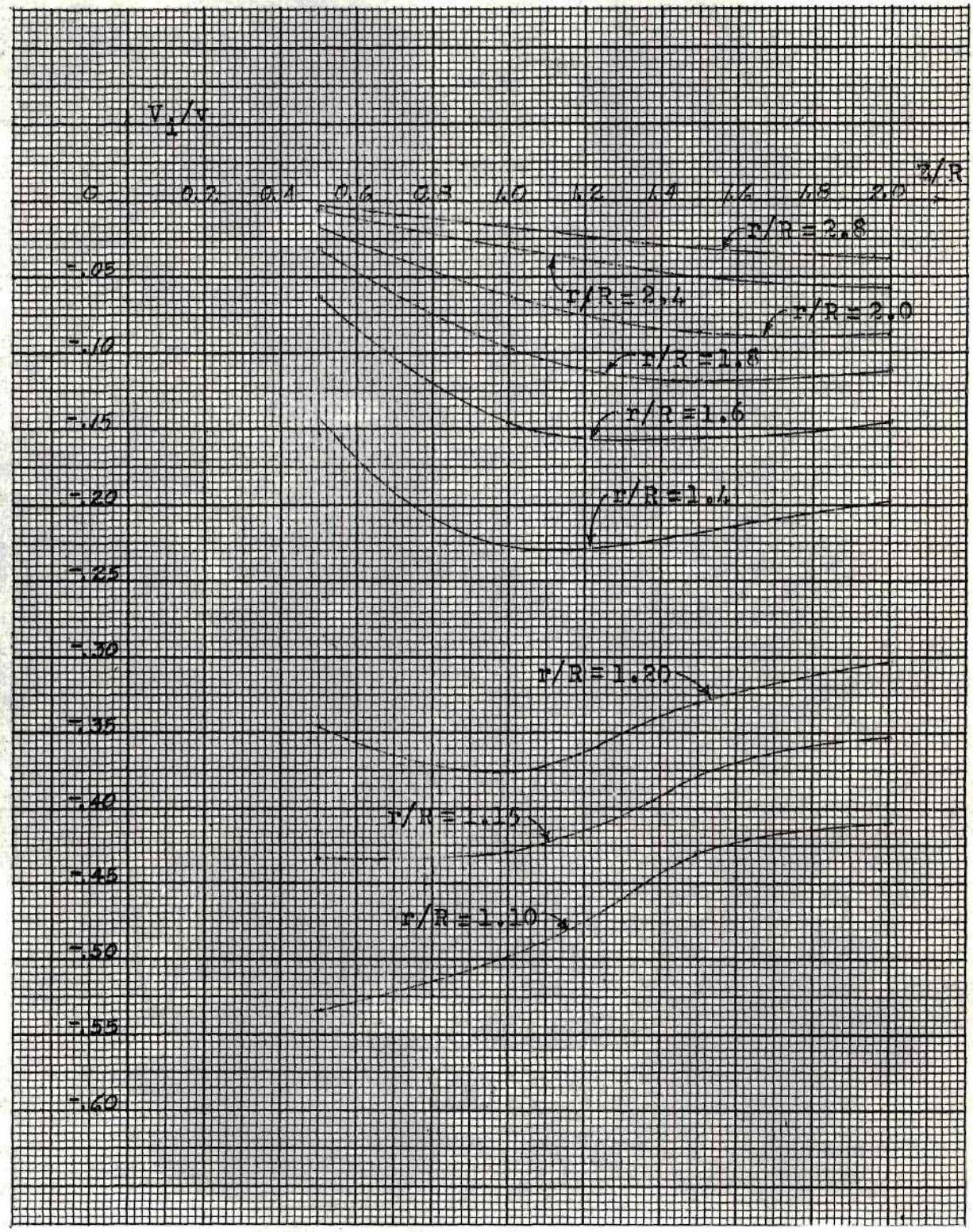

(b) For h/R = - 0.2

Figure 9. Continued

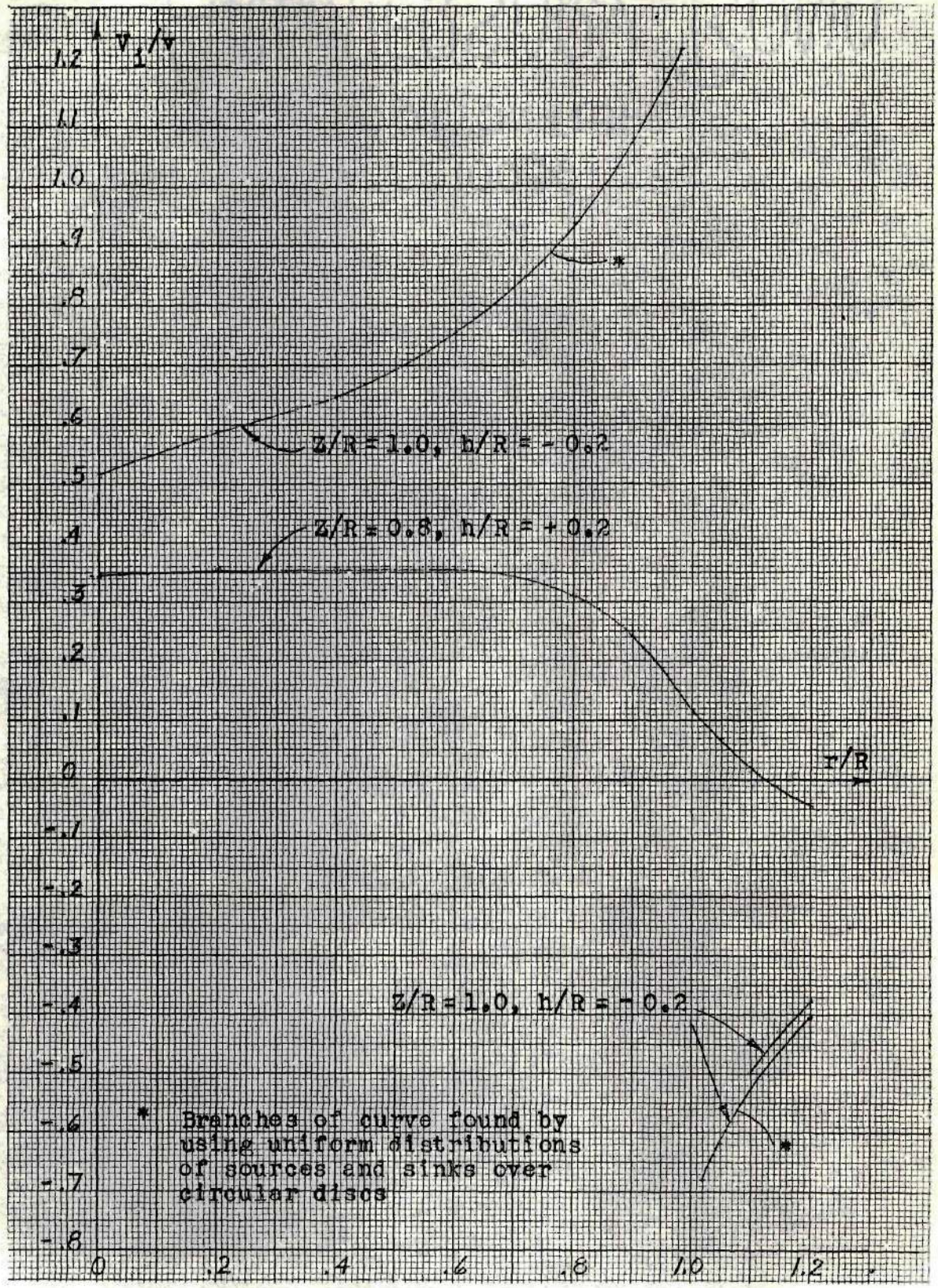

Figure 10. Variation of Nondimensional Normal Component of Induced Velocity Along the Radius For Z/R = 1.0, h/R = - 0.2, and For Z/R = 0.8, h/R = + 0.2

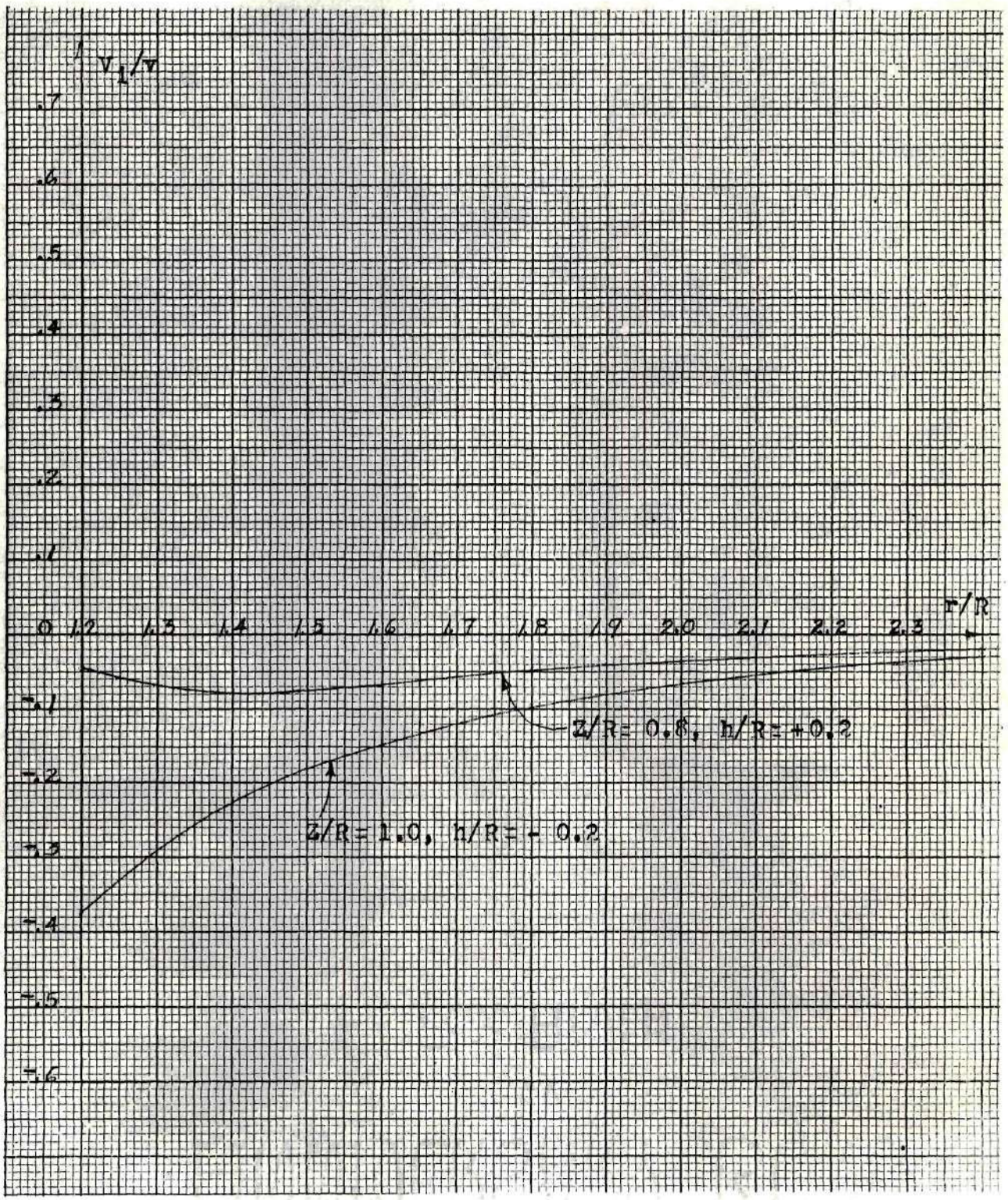

Figure 10. Continued

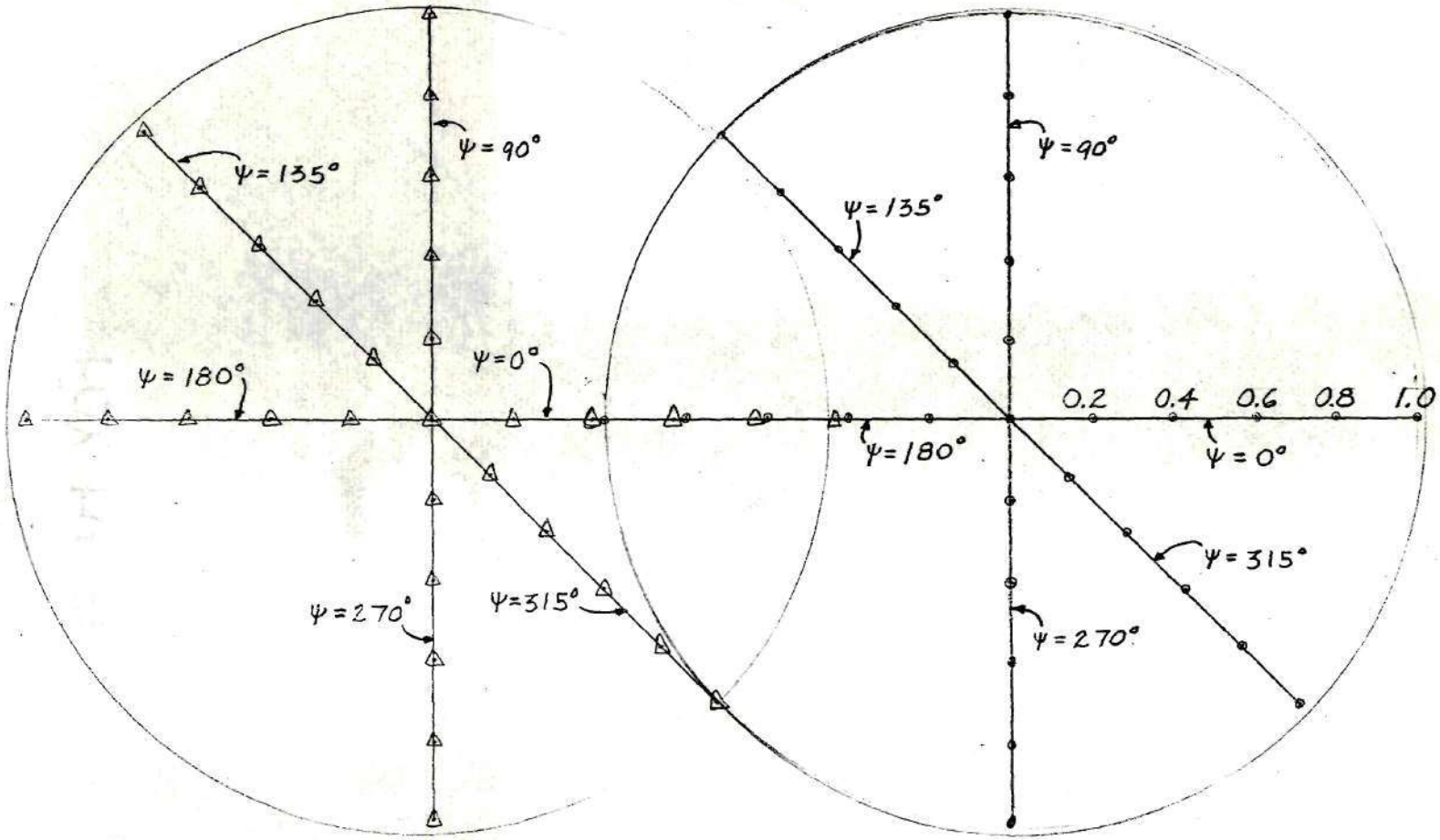

Figure 11. Plan View of Rotors of Tandem-rotor Helicopter Showing Location of Points For Which the Nondimensional Interference Induced Velocity is Calculated

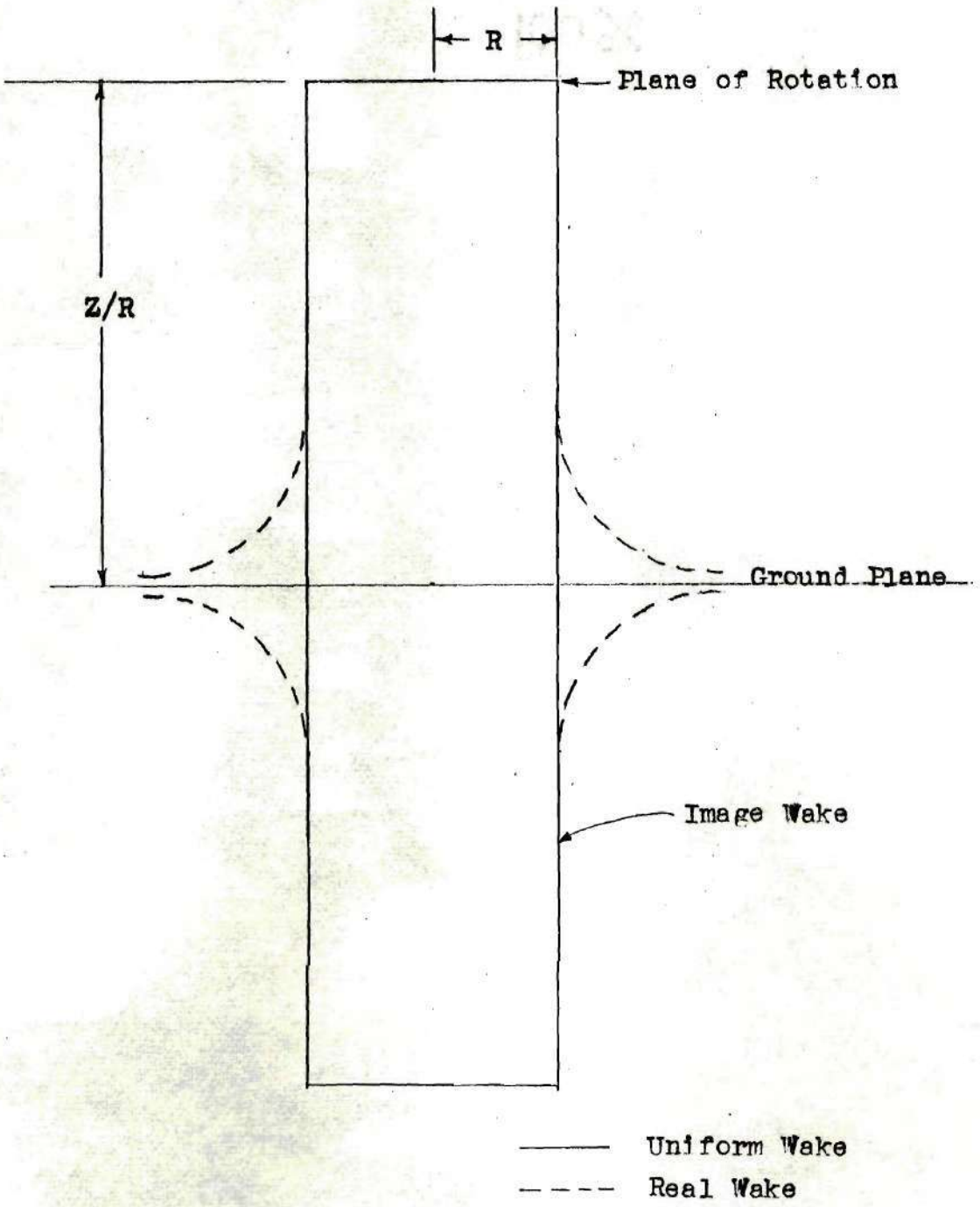

Figure 12. Comparison of the Shape of a Real and a Uniform Wake

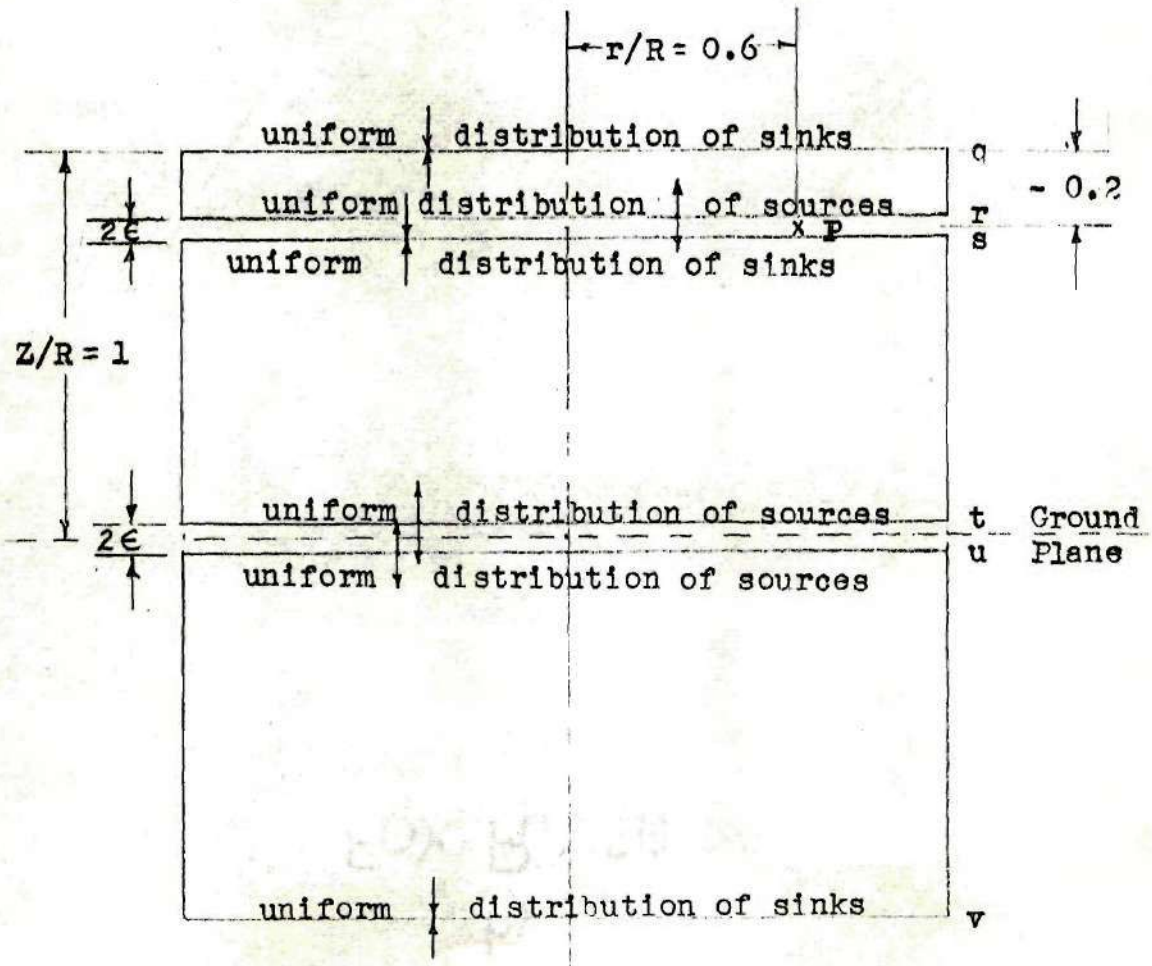

Figure 13. Cross-section of the Wake Showing Three Finite Uniform Vortex Cylinders the Flow Fields of Which are Duplicated by the Superposition of Uniform Distributions of Sources and Sinks Over Circular Discs

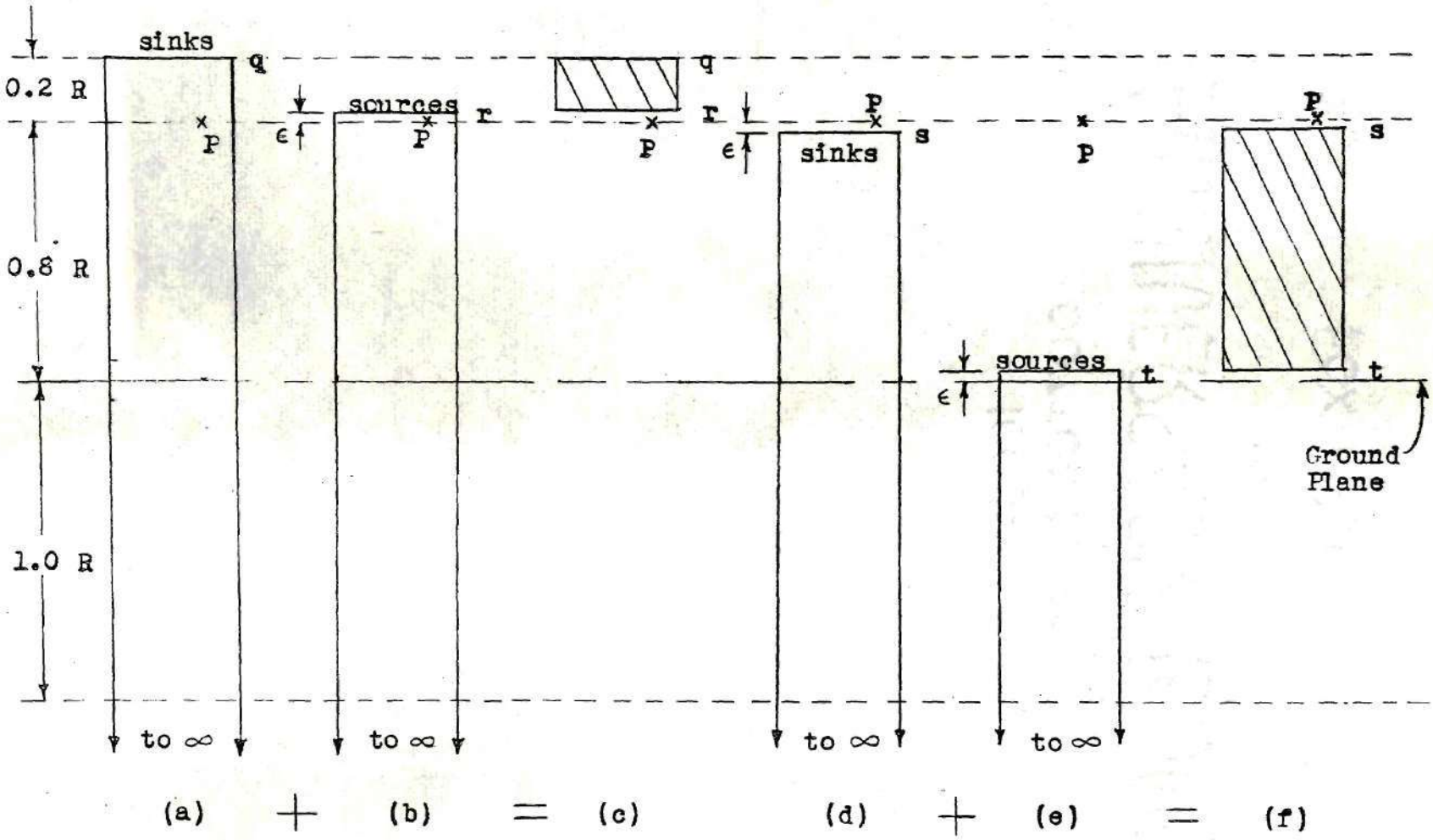

Figure 14. Diagram Showing the Superposition of Uniform Distributions of Sources and Sinks Such That They Are Equivalent to Three Finite Uniform Vortex Cylinders

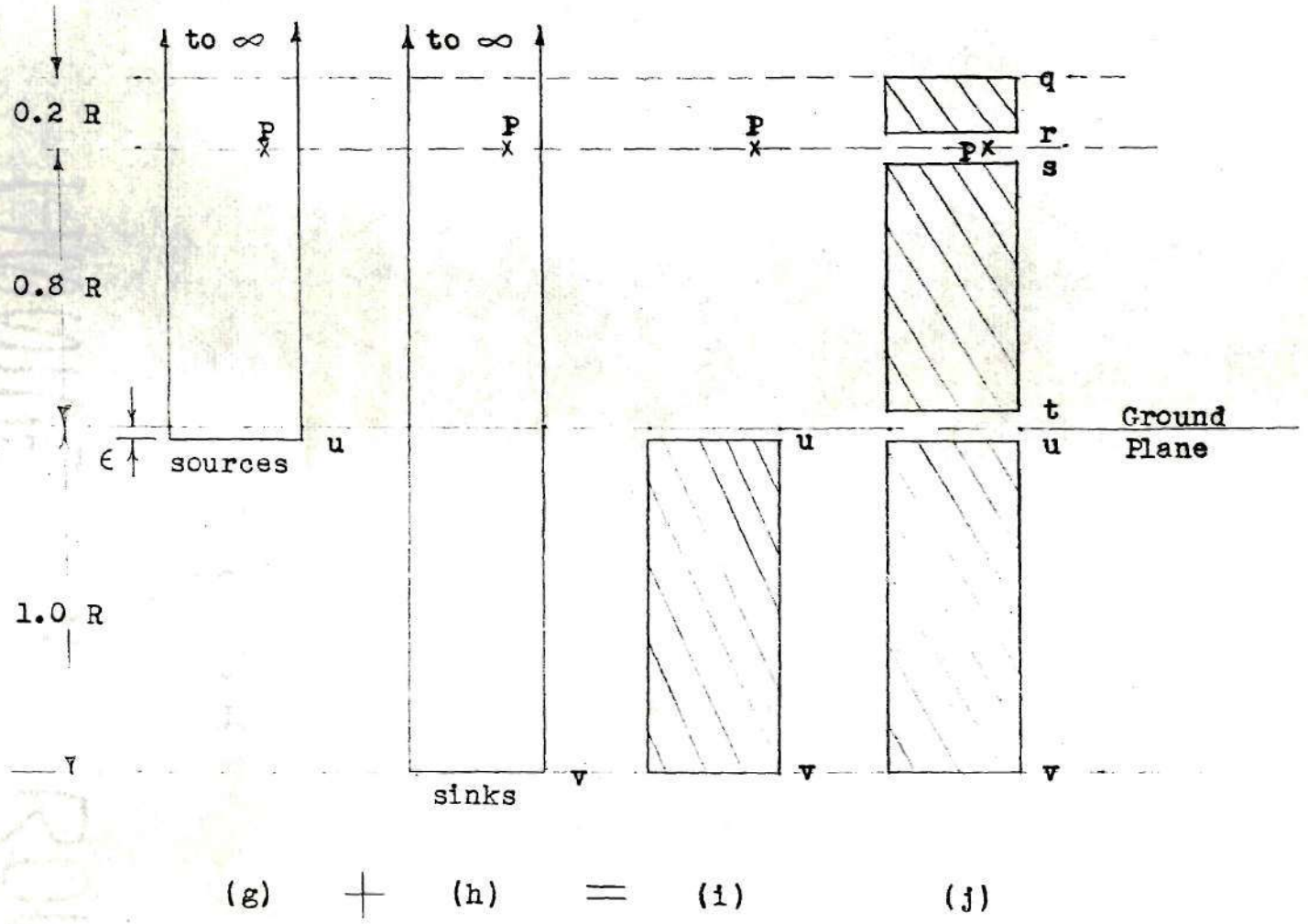

Figure 14. Continued

BIBLIOGRAPHY

1. Knight, Montgomery, and Hefner, Ralph A., Analysis of Ground Effect On the Lifting Airscrew, National Advisory Committee For Aeronautics, Technical Note No.835, 1941.

2. Castles, Walter, Jr., Durham, Howard L., Jr., and Kevorkian, Jiriar, Normal Component of Induced Velocity For Entire Field of a Uniformly Loaded Lifting Rotor With Highly Swept Wake As Determined By Electromagnetic Analog, National Advisory Committee For Aeronautics, Technical Note No. 4238.

3. Kuchemann, Kietrich, and Weber, Johanna, Aerodynamics of Propulsion, New York : McGraw Hill Book Company, 1953, p. 52-57, 319-320.